Formation of IIAB iron meteorites

John T. Wasson *, Heinz Huber, Daniel J. Malvin

Institute of Geophysics and Planetary Physics, University of California, Los Angeles, CA 90095-1567, USA

Abstract

Group IIAB is the third largest group of iron meteorites and the second largest group that formed by fractional crystallization; many of these irons formed from the P-rich portion of a magma consisting of two-immiscible liquids. We report neutron-activation data for 78 IIAB irons. These confirm earlier studies showing that the group has the largest known range in Ir concentrations (a factor of 4000) and that slopes are steeply negative on plots of Ir vs. Au or As (or Ni). High negative slopes imply relatively high distribution coefficients for Ir, Au, and As (but, with rare exceptions, remaining less than unity for the latter). IIAB appears to have had the highest S contents of any magmatic group of iron meteorites, consistent with its high contents of other volatile siderophiles, particularly Ga and Ge. Large fractions of trapped melt were present in the IIAB irons with the highest Au and As and lowest Ir contents. As a result, when these irons crystallized, the D_{Au} and D_{As} values can, with moderate accuracy, be estimated to have been roughly 0.53 and 0.46, respectively. These low values imply that the initial nonmetal (S + P) content of the magma was much lower than 170 mg/g, as estimated in earlier studies; our estimate is 75 mg/g. Our results are consistent with an initial P/S ratio of 0.25, similar to the ratio estimated for other magmatic groups. There is little doubt that incompatible S-rich and P-rich metallic liquids were involved during the formation of group IIAB. After 20% crystallization of our assumed starting composition the two-liquid boundary is encountered (at 72 mg/g S and 18 mg/g P). Initially the volume of S-rich liquid is very small, but continued crystallization increased the volume of this phase and decreased its P/S ratio while increasing this ratio in the P-rich liquid. Most crystallization of the IIAB magma would have occurred in the lower, P-rich portion of the core. However, metal was still a liquidus phase at the top of the core and, because both the immiscible liquids would have convected, they may have approached equilibrium throughout the very limited crystallization of the magma recorded in group IIAB. All IIAB irons contain trapped melt, and this melt will have had very different compositions depending on whether the liquid is S-rich (at the outer solid/liquid interface) or P-rich (at the inner interface). The P/S ratio in the melt trapped in the Santa Luzia iron is about 0.6 g/g, consistent with our modeling of Ir–Au and Ir–As trends implying that Santa Luzia formed in the lower, P-rich portion of the core after about 48% crystallization of the magma. Because the liquids were in equilibrium, the point at which immiscibility first occurred is not recorded by a dramatic change in the trends on element–Au diagrams; the main compositional effect is recorded in the P/S ratio of the trapped melt. The high-Au (>0.8 µg/g) irons for which large sections are available all contain skeletal schreibersite implying a relatively high (>0.3 g/g) P/S ratio; none of these irons could have crystallized from the S-rich upper layer of the core.
© 2006 Elsevier Inc. All rights reserved.

1. Introduction

Group IIAB is the third largest group of iron meteorites and the second largest group that formed by fractional crystallization. It has a very large (4000, earlier stated to be 5000) range in Ir and Ir–Ni arrays have high negative slopes, the highest in any group (Wasson, 1969). Group

IIAB was originally divided into IIA irons with hexahedrite structures and IIB irons with coarsest-octahedrite structures. There was a hint of a change of slope on Ga–Ni and Ge–Ni diagrams near the hexahedrite–octahedrite boundary. It later became clear that there is no compositional hiatus and no accrued gain in attempting to define a boundary between IIA and IIB.

Although instrumental-neutron-activation-analysis (INAA) data have been published for several IIAB irons (e.g., Wasson et al., 1989), this is the first comprehensive study of the group using this technique. We present data

---

* Corresponding author. Fax: +1 310 206 3051.
  E-mail addresses: jtwasson@ucla.edu (J.T. Wasson), djmalvin@ca.rr.com (D.J. Malvin).

for 78 independently cataloged IIAB irons as well as for additional specimens of IIAB irons that were originally cataloged separately but are now believed to be fragments of the same shower (e.g., Pirapora and Angra dos Reis).

Wasson (1999) noted that the IIIAB Ir–Au and Ir–As trends could be explained by a combination of fractional crystallization and equilibrium melt trapping. Wasson and Richardson (2001) used the same approach to model the compositions of IVA irons. In this paper we apply this approach to understanding the formation of the IIAB irons.

In a metallic magma the solid/liquid distribution coefficient D for S is very small; in our studies (e.g., Wasson and Richardson, 2001) we assume the D_S value to be 0.005 g/g (all D values in this paper are in mass units). As a result, S remains almost quantitatively in the melt during the crystallization of metallic magmas. Because so little S enters into the crystallizing metal, exsolution of S from the metal at low temperatures is negligible. Thus the centimeter-size FeS nodules that are common in iron meteorites reflect the presence of trapped melt.

During the past three decades solid/liquid distribution coefficients for metallic systems have received considerable study, particularly in the Drake lab at the University of Arizona. Reviews have been published by Jones and Malvin (1990) and by Chabot and Jones (2003). Most D values are strongly dependent upon the nonmetal (S, P, and C) concentrations in the melt.

For the siderophile elements one can estimate the initial composition of the molten core by constructing fractionation models that approximately match the general elemental trends, commonly plotted as log element–log Ni or log element–log Au diagrams (e.g., Wasson and Huber, 2006). The initial composition of the melt, obtained by fitting the first-formed solids, is the mean composition of the core.

It is much more difficult to estimate the concentration of nonmetals in the core. Because S is the most abundant nonmetal, most effort has been spent on attempting to assess its concentration. Esbensen et al. (1982) and Wasson (1999) modeled the large variations in trapped melt observed among the different large masses of the Cape York iron to estimate the S concentration in the IIIAB core. Haack and Scott (1993) took a different approach; they (largely) accepted the fitted algorithm of Jones and Malvin (1990) linking the D values of several elements (especially Ge, Ir, and Ni), and chose an initial S concentration for IIIAB that best fit the observed trends. Chabot (2004) followed the same procedure using the Chabot and Jones (2003) algorithm and included additional elements including Au and Ga. We discuss these two approaches, and make the case for adjusting the D values within allowable ranges in order to maximize the ability to fit the iron meteorite trends in a plausible way.

At moderately high concentrations of S and P two-immiscible metallic melts form. If, as Chabot (2004) proposed, the IIAB initial magma contained 170 mg/g S (actually 170 mg/g nonmetals with major S and minor P), the discussions of Ulff-Møller (1998) and Chabot and Drake (2000) indicate that the magma should separate into immiscible P-rich and S-rich liquids. Compositions having lower initial nonmetal contents eventually evolve into the two-liquid field. We examined the chemical and mineralogical compositions of the irons to determine whether there is evidence for this having occurred.

Group IIAB is the only major iron meteorite group for which no oxygen-isotopic data are available. We therefore have no straightforward method to link the IIAB group to a particular kind of chondritic parental materials. A few rare oxides have been reported (Frondel and Klein, 1965; Buchwald, 1975) thus this key taxonomic parameter will surely become available during the next several years.

2. Analytical techniques and samples

We determined 13 elements (12 plus Fe) in metal by instrumental neutron-activation-analysis (INAA) in replicate analyses; data for Fe are used for internal normalization. Most meteorites were analyzed two or three times to improve the precision. The procedures are those given by Wasson et al. (1989) except for two minor changes. The mean sample thickness is now 3.0 instead of 3.2 mm, and we now apply small (generally in the range 0.95–1.05) sample-specific corrections to make the Ni values in the first count agree better with those from the third and fourth counts (which are corrected to make Fe + Ni = 990 mg/ g). We then choose a correction factor for the second count that is intermediate between that for the first and the mean corrections in the third and fourth counts.

Concentrations of Ge and the (sparse) data for Sb were determined by radiochemical neutron-activation-analysis (RNAA). We do not currently carry out RNAA studies of iron meteorites. Our INAA Ge data for IIAB irons typically have high uncertainties, with 95% uncertainties about 7–10% for the mean of two replicates; Sb uncertainties are several times larger and concentrations are below our INAA detection limit of about 120 ng/g in most samples. We have chosen not to report these less precise data because more precise RNAA Ge data are available for ∼90% and RNAA Sb data available for ∼20% of the studied meteorites.

Although the INAA data were gathered over almost three decades, significant improvements in the quality were achieved starting in 1986. As a result, some meteorites were restudied and the recent analysis given double weight in the determination of the mean. In most meteorites we had previously determined Ni by atomic-absorption spectrophotometry; in these cases the Ni means were calculated treating the previous mean as an additional replicate. We have now recalculated older analytical runs to incorporate these more sophisticated correction procedures. In the oldest runs we did not yet use Filomena as a standard; instead we irradiated aliquots of standardized solutions, a technique that was less reproducible. In our recalculations we have used newer analyses of some of the irons in these ear-

lier runs to restandardize them; most of the revisions are smaller than 5% relative.

To facilitate locating meteorites in the diagrams, in Table 1 (also published as Table EA1 in the electronic annex) we list the mean compositions of IIAB irons in order of increasing Au concentration. Individual analyses are listed alphabetically in Table A1 (also published as Table EA2) and Table EA3 together with the irradiation dates. Some of the means listed in Table 1 differ from published values, mainly because of the minor changes in calibration.

We estimate relative 95% confidence limits on the listed means to be 1.5–3% for Co, Ni, Ga, and Ir (concentrations >0.1 µg/g) and Au, 4–6% for As, Ge, and Sb (the latter two by RNAA), 7–10% for W (values >0.3 µg/g), Re (>50 ng/g), Ru (>4 µg/g) and Pt (>2 µg/g). Because much of the Cr is in minor phases (mainly chromite and daubreelite) sampling errors result in relative confidence limits on the mean >10%. In addition, there is an Fe interference in the determination of Cr resulting from the $^{54}Fe(n, \alpha)^{51}Cr$ fast-neutron reaction; our somewhat uncertain estimate of the level of interference is 6 µg Cr per gram of Fe (Wasson and Richardson, 2001). Our data were not corrected for this interference.

In runs carried out during the past two decades we used three INAA standards, two of which are IIAB irons the Filomena specimen of the North Chile shower and a Coahuila specimen off an undetermined mass of this shower. We find Filomena to be a very uniform iron, and thus well suited to be a standard. Only Cr shows moderate scatter (a standard deviation of about 17% relative). Coahuila is more variable in Cr (relative standard deviation 35%) but is otherwise adequately uniform for use as a standard. Our third standard is the NBS steel NBS809B; the Mn content of NBS is so high that we cannot include it in the first count several hours after the end of an irradiation. We list the analyses of these standards for the period 1994–2005 in Table EA4 in the electronic annex. We also list means and standard deviations; the latter are unrepresentatively low because the same samples were used as standards.

In Table 4 we list the results of a study of samples from a 10-cm bar of the Santa Luzia iron provided us by the Smithsonian Institution. Included among the 12 samples are one each (mainly) consisting of schreibersite and troilite. These Santa Luzia samples were not analyzed in duplicate.

There are several IIAB irons that were initially cataloged under different names. The best known are the numerous North Chile hexahedrites (Schaudy et al., 1972). Two irons (Central Missouri and Ponca Creek) are paired with Ainsworth and Angra dos Reis (iron) is paired with Pirapora. We also have questions about the three new irons Dutch Flat, Elqui and "Fredericksburg" which are unresolvable from Sikhote-Alin, Mejillones and Richland, respectively. Our replicate data for these irons are given in Table A1 discussed in the Appendix. Also listed in Table A1 are our analyses of different structural regions (H and Ogg) of the Old Woman iron that were provided us (by

Roy Clarke) for study, but which proved to be unresolvable compositionally.

Buchwald (1975) noted that Iredell was found on a road and speculates that it might be a piece of El Burro despite the fact that it was found 450 km NE of the latter. Our data show that the two irons differ by 50% in Ir and 15% in Au; they are not parts of the same shower. We interpret the compositional data to show that Iredell is not paired with any other IIAB iron analyzed by us.

We minimize contamination of our samples by careful preparation and by a brief etching with a dilute mix of HCl and HNO_3 following the irradiation. We nonetheless found that a few samples were contaminated; contamination is commonly indicated by disagreement between replicates and a concentration that is inconsistent with the observed concentration of closely related elements. The As concentrations in our samples of Cincinnati and Pima County were so contaminated that we do not report a mean in Table 1 nor do we plot As on diagrams. A few samples showed minor contamination with Au; we suspect that contamination mainly occurred during storage together with mineral specimens by dealers or museums.

The high content of nonmetallic inclusions creates a sampling problem in the high-Au members of group IIAB. As discussed in more detail later, these commonly contain large skeletal schreibersite surrounded by swathing kamacite. Clarke and Goldstein (1978) showed petrographic evidence indicating that, with decreasing temperatures, Ni and Fe exchange between schreibersite and kamacite results in increases in Ni in the schreibersite and decreases in the adjacent kamacite. Our analytical goal is to provide accurate data for the metal in the investigated meteorites, but it is sometimes difficult to completely avoid inclusions, resulting in somewhat low concentration data. Equally serious, to accurately model the chemical evolution of the group one needs to know whole-rock compositions; the S and P contents of whole rocks are never well determined and frequently not determined at all, thus our metal concentration data only provide approximations of whole-rock values. Because massive schreibersite is so common in IIAB there is no doubt that whole-rock Ni contents are appreciably higher than those we report.

The Ir range in the IIAB irons is the largest among the magmatic groups. It ranges from 48 µg/g in Scottsville and 47 µg/g in Negrillos to 0.012 µg/g in Sao Juliao and Silver Bell. We believe that the somewhat higher concentration of Ir (and those of most other siderophiles) in the Avce iron is spuriously high. Because the main mass of this observed fall is on exhibit and considered an outstanding showpiece, we could only obtain a very thin sample that had been deeply etched. We suspect that this etching selectively removed Fe, and thus resulted in the enhancement of all siderophiles having high taenite/kamacite concentration ratios. In Wasson (1969) and several later papers our group stated that the Ir range was 5000 in group IIAB. However, because our newer, more precise INAA data show a lower Ir concentration in Negrillos and because we suspect that

Table 1
Mean compositions of 78 IIAB iron meteorites

Meteorite	Cr	Co	Ni	Cu	Ga	Ge	As	Sb	W	Re	Ir	Pt	Au	P
Bennett County	92	4.46	54.0	131	56.5	179	3.53		3.62	4540	43.6	31.8	0.474	2.3
Negrillos	92	4.49	52.5	136	57.5	179	3.55		3.72	4894	47.4	33.1	0.477	2.2
Patos de Minas (hex.)	<100	4.47	53.2	142	58.4	170	3.62	36	3.62	4928	46.3	36.5	0.486	2.0
Sierra Gorda	144	4.49	55.4	156	60.3	169	3.64		3.86	4890	43.9	35.9	0.488	2.3
Scottsville	86	4.48	53.7	141	60.4	172	3.79		3.91	5210	47.9	35.7	0.492	2.1
Murphy	64	4.48	53.3	143	60.4	186	3.93		3.81	3880	37.8	34.2	0.506	3.4
Bruno	157	4.51	53.6	124	58.0	185	3.86		3.48	2835	30.2	32.1	0.509	2.0
Forsyth County	63	4.44	55.4	136	60.4	176	3.90		3.69	4044	40.4	35.1	0.510	2.1
Edmonton (Canada)	89	4.51	53.1	149	59.5	172	3.77		3.61	2928	31.5	35.6	0.513	2.0
Avce	161	4.46	54.5	148	58.8	182	4.02		4.00	7309	59.5	39.4	0.514	2.0
Crow Peak	128	4.46	57.2	138	57.8	167	3.72		3.40	3365	36.5	34.5	0.515	
Allan Hills AA78100	77	4.48	54.9	141	58.3	188	3.87	43	3.50	2829	30.0		0.522	2.0
San Francisco d.M.	116	4.49	55.1	138	60.2	183	4.11		3.47	2770	28.5	31.0	0.522	2.0
Boguslavka	70	4.48	54.6	140	59.2	180	4.01		3.33	2405	25.9	31.5	0.523	3.0
Pirapora	99	4.51	54.1	137	58.9	189	3.83		3.51	3070	31.0	34.4	0.523	2.0
Angra dos Reis	107	4.49	53.4	134	56.9	188	3.89		3.50	2790	30.8	33.2	0.524	
NWA2678	106	4.47	54.5	134	58.0	163	3.83		3.17	2370	25.7	30.6	0.527	2.5
Holland's Store	55	4.51	54.5	135	59.9	182	4.01		3.46	1545	18.4	29.2	0.529	
Guadalupe y Calvo	68	4.47	54.0	136	60.2	182	3.91	48	3.52	4520	42.6	37.2	0.534	3.0
Okahandja	86	4.53	55.9	144	57.8	193	4.03		3.08	845	10.9	29.9	0.537	
Smithonia	69	4.52	56.0	122	59.3	187	3.94		3.65	3802	38.3	35.1	0.537	2.0
Cosmo Newberry	83	4.61	54.3	116	59.3	180	4.08	57	3.55	2100	23.2	30.6	0.538	2.0
Cincinnati	74	4.53	54.5	145	58.2	178			3.43	1720	20.3	30.0	0.540	
Squaw Creek	65	4.35	54.9	126	57.8	182	4.21	47	3.21	952	10.6		0.544	2.8
Anyujskij	56	4.47	55.1	138	59.5	172	4.09	41	3.18	1410	14.4	26.0	0.546	
Coahuila	214	4.54	55.0	141	58.5	180	4.20		3.15	1290	16.1	28.3	0.546	2.0
Siratik	61	4.45	56.6	136	57.2	188	4.11	51	3.09	958	11.2		0.550	
Yarroweyah	216	4.51	56.3	148	60.8	171	4.20		3.29	1510	16.0	29.8	0.552	2.0
Muenatauray	132	4.52	53.9	130	57.5	183	4.08		3.06	1046	12.9	27.6	0.553	
Keen Mountain	101	4.54	54.9	139	59.3	182	4.32		3.13	1004	12.1	25.8	0.554	
Carver	77	4.46	56.8	138	59.4	184	4.08		3.06	863	11.3		0.555	
Chico Mountains	58	4.52	54.1	133	58.4	176	4.29		2.78	622	8.41	24.4	0.558	3.3
Cedartown	96	4.56	54.5	132	59.5	181	4.35		2.88	830	10.2	25.7	0.559	3.0
Indian Valley	94	4.49	54.6	144	58.5	174	4.32		3.01	954	11.6	28.6	0.560	2.7
NWA3202	138	4.51	56.1	131	58.9		4.14		2.82	853	11.4	28.4	0.570	
Braunau	73	4.52	55.0	141	59.7	183	4.36		3.16	877	11.3	30.4	0.572	2.4
Fredericksburg	91	4.58	55.2	134	58.4		4.38		2.83	666	8.44	25.2	0.575	
Calico Rock	77	4.51	55.6	135	59.0	186	4.32		3.01	741	9.27	26.4	0.578	
Pima County	71	4.56	56.5	149	60.6	182			2.96	663	8.80	26.5	0.586	2.5
Richland	36	4.56	55.3	125	59.9	181	4.65		2.75	660	8.52	26.6	0.586	2.4
Wathena	58	4.53	54.6	136	59.0	184	4.40		2.85	599	8.02	24.7	0.586	2.7
Okano	233	4.55	56.0	138	59.9	180	4.34		3.03	859	11.4	25.5	0.587	
Locust Grove	69	4.54	56.1	134	59.7	180	4.64		2.74	566	7.46	22.8	0.592	2.5
El Mirage	76	4.58	55.4	137	58.6	185	4.52		2.78	405	5.93	23.9	0.593	
Gressk	41	4.58	55.7	137	60.4	177	4.58		2.76	561	7.48	24.3	0.598	2.8
Hex River Mountains	123	4.57	55.8	131	59.1	181	4.65		2.48	279	4.13	22.8	0.609	2.5
North Chile	45	4.54	56.0	131	58.5	177	4.81		2.58	212	3.43	21.8	0.617	3.0
Walker County	152	4.60	55.3	135	58.6	189	4.86		2.50	233	3.27	22.0	0.623	2.8
Uwet	73	4.59	56.6	136	59.4	182	4.94		2.39	192	2.77	18.7	0.629	2.5
Kopjes Vlei	78	4.56	55.9	141	59.8	182	4.96		2.46	225	3.43	21.2	0.630	3.0
Lombard	46	4.58	55.0	129	59.0	177	5.09		2.32	196	2.68	20.7	0.645	2.8
Chesterville	201	4.61	56.3	136	59.4	178	5.22		2.26	130	1.77	19.8	0.654	3.0
Park City	66	4.56	58.9	127	57.0	178	5.15		2.24	151	2.31	21.3	0.661	
Elqui	590	4.57	59.8	136	59.3	167	5.23	65	2.16	140	1.94	17.3	0.662	
Mejillones	178	4.62	54.9	130	59.7	177	5.16		2.22	130	1.92	19.2	0.663	3.3
Old Woman	47	4.66	55.4	125	57.0	184	5.48		2.05	44.7	0.830	15.2	0.689	
Navajo	37	4.69	54.9	126	58.3	181	5.96		1.89	28.2	0.513	14.6	0.719	3.0
Mount Joy	52	4.66	57.8	133	60.5	182	6.22		1.61	22.8	0.423	12.9	0.779	2.8
Jerslev	38	4.79	55.4	124	57.7	168	6.99	59	1.26	<100	0.234	9.9	0.830	3.5
Bilibino	36	4.71	59.9	127	59.7	176	7.43	66	1.39	<60	0.121	9.3	0.860	
Smithsonian Iron	38	4.85	55.5	109	54.0	165	7.38		1.10	3.89	0.065	7.7	0.873	2.5
Sandia Mtns.	44	4.75	57.9	130	57.7	170	7.62		1.24	8.44	0.136	8.8	0.879	4.0
El Burro	38	4.73	58.8	121	54.8	168	7.27		1.03	<23	0.077	8.4	0.887	3.2

Table 1 (*continued*)

Meteorite	Cr	Co	Ni	Cu	Ga	Ge	As	Sb	W	Re	Ir	Pt	Au	P
Nenntmannsdorf	23	4.80	59.9	130	56.7	172	7.74	87	1.08	<49	0.077	8.0	0.903	3.0
Iredell	28	4.78	58.9	123	57.1	163	8.36		0.92	<30	0.045	7.1	0.970	2.0
Veevers	26	4.81	57.2	117	56.0	160	8.74		0.89	<20	0.029	4.9	0.998	
Dutch Flat	38	4.89	57.8	112	55.5	132	9.04		0.82	<40	0.021	5.2	1.030	5.0
Sikhote-Alin	31	4.79	60.3	117	53.7	158	9.40		0.74	<30	0.024	5.5	1.049	
ElephMo EET83245	22	4.86	60.4	119	55.8	157	9.71	86	0.74	<100	0.026		1.065	4.6
Ainsworth	32	4.84	61.4	115	54.0	142	9.25		0.64	1.5	0.022	4.1	1.068	7.0
Foum Zguid	22	4.97	58.1	113	55.5	153	9.91		0.72	<40	0.021	5.3	1.078	
Derrick Peak	28	4.76	63.6	113	52.9	135	9.31	94	0.56	<20	0.018	4.1	1.084	
Lake Murray	26	5.00	60.3	106	52.7	141	10.2		0.56	<25	0.015	2.7	1.087	5.0
NWA3201	15	5.11	52.1	118	51.6	130	11.1		0.54	<33	0.017	3.7	1.089	
Silver Bell	15	5.26	58.9	98	45.7	111	12.3		0.36	<30	0.012	1.9	1.252	8.0
Summit	17	4.84	65.5	116	50.4	115	11.4		0.42	<30	0.014	1.9	1.267	5.0
Santa Luzia	15	5.05	60.4	107	46.2	110	11.7	100	0.33	0.714	0.013	2.9	1.290	9.0
Sao Juliao	16	5.19	57.8	94	45.8	106	12.5	79	0.40	0.765	0.012	2.3	1.350	9.0

Concentrations are μg/g except P, Co, and Ni (mg/g), and Sb and Re (ng/g). P data are from Buchwald (1975). Re data <50 ng/g (and not upper limits) are from Cook et al. (2004).
North Chile data are for the Filomena specimen.

the Avce value is too high because of sample treatment, we feel that 4000 represents a more accurate estimate of the IIAB Ir range. Note that the ranges in Os and Re are still larger, ~10,000 and ~6000, respectively (Cook et al., 2004).

We used modal integration to determine the S and P contents of several large sections of IIAB irons. These are tabulated together with data extracted from Buchwald (1975) in Table 2. With the exception of Carver, all of our data are based on photographic images. There is an important difference between our P values (bold in Table 2) and those of Buchwald; our values reflect only massive schreibersite whereas Buchwald reported bulk P values that include the small schreibersite inclusions called rhabdites as well as P dissolved in the metal. Our Carver specimen has suffered shock shear and FeS melting, with the result that FeS boundaries are frequently ragged and less sharp than optimum for integration.

3. Results: element–Au trends in group IIAB

Scatter diagrams for 12 elements plotted against Au are shown in Figs. 1 and 2. In Fig. 1 we show data for six elements that are commonly used for taxonomy. As already well known, the volatile elements Ga (Fig. 1a) and Ge (Fig. 1b) have high concentrations in group IIAB; for Au <0.9 μg/g there is no resolvable slope in either distribution, an observation potentially useful for assessing the initial nonmetal content of the magma. High-S contents are expected to yield D_{Ge} and D_{Ga} values ≫1 (e.g., Chabot, 2004).

In all iron meteorite groups the As and Au concentrations are closely related; log As–log Au diagrams show slopes slightly greater than unity and very limited scatter indicating small analytical and sampling errors (Fig. 1c). Our sparse RNAA Sb data show that the Sb–Au trend (Fig. 1d) is similar to the As–Au trend, implying near-iden-

Table 2
Modal estimates of P and S in IIAB irons by Buchwald (1975) and by us (bold; see text) based on large sections (and one Santa Luzia shown in Fig. 3)

Meteorite	Area (cm²)	P (mg/g)	S (mg/g)	Ir (μg/g)	G	Trap fr.
Ainsworth	120[b]	7.0	1.4	0.024	48	28
Braunau	~200?	2.4	0.8	11.3	15	8
Carver	468		1.7	11.3	14	3
Coahuila	720		0.85	16.1	11	4
Derrick Peak	420	3.5[a]	2.6	0.018	46	30
Guadalupe y Calvo	860		1.1	42.6	2	13
Hex River Mtns.	1680		1.8	4.13	28	2
Keen Mountain	225	2.3	3.0	12.1	14	7
Mount Joy	4700		1.3	0.423	39	7
North Chile	1600	3.0	1.0	3.43	28	3
Santa Luzia (Rio)	1800	6.6[a]	12.3	0.013	48	70
Santa Luzia-RSC	75	6.1[a]	4.8	0.013	48	70
Sikhote-Alin	>300	4.6	2.8	0.024	48	28

The Ir concentration is given as a rough measure of the degree of crystallization G; the penultimate column gives a better estimate based on our fits to the Ir–Au and Ir–As data. The final column gives the trapped fraction based on the Ir–Au and Ir–As fits. See text for details.
[a] As massive schreibersite; P values by Buchwald (1975) include rhabdites and metal.
[b] The combined areas of Ainsworth, Central Missouri and Ponca Creek at the Smithsonian Institution are 340 cm² but it appears that the FeS content quoted by Buchwald is based only on a 120 cm² section of Ainsworth.
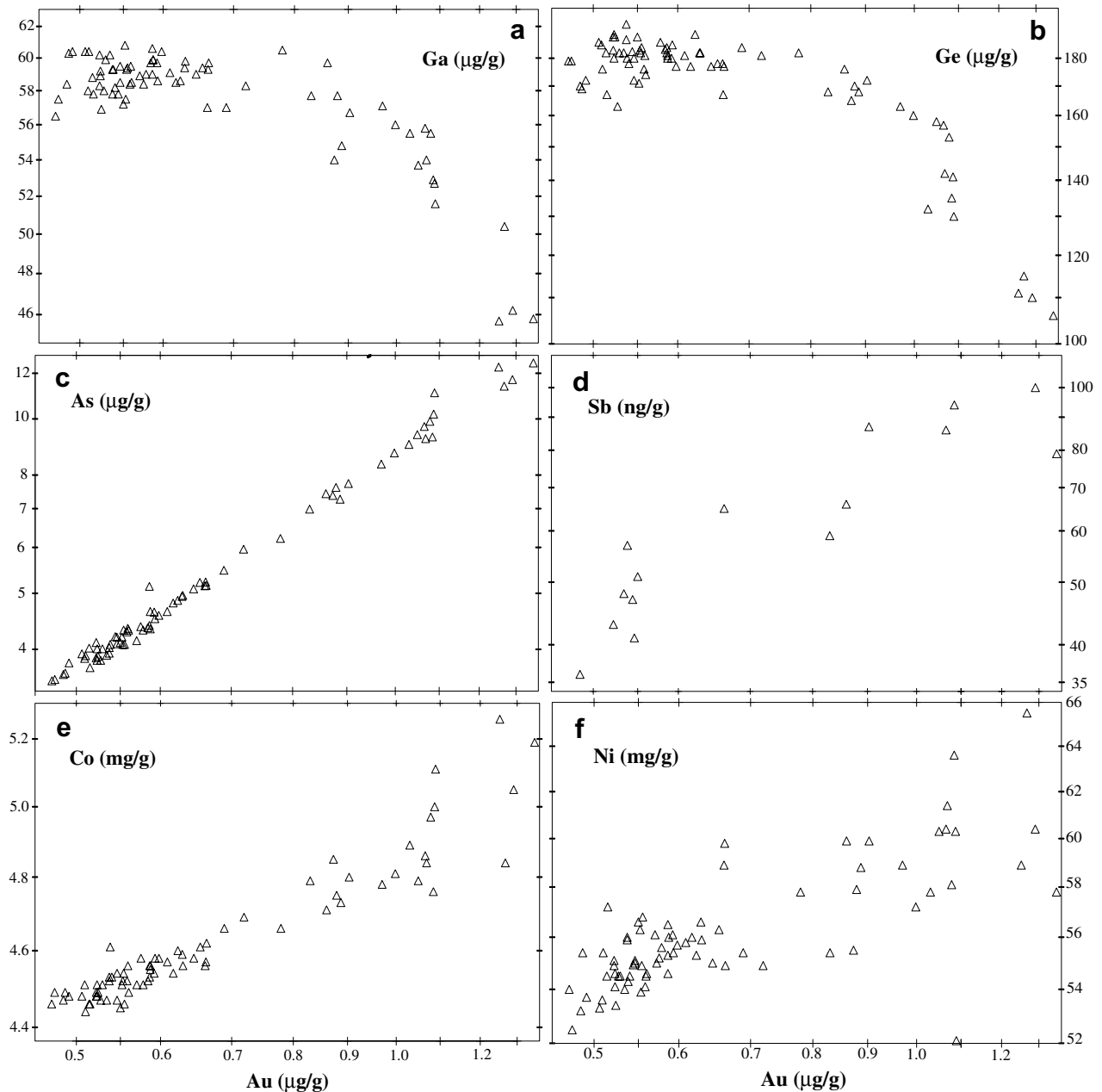
Fig. 1. Log-element, log-Au diagrams for six elements used for taxonomy; two (Ga and Ge) show little change across the group and four (As, Sb, Cu, and Ni) show positive trends indicating incompatibility with solid metal during crystallization of the IIAB magma.

tical behavior during crystallization; there is, however, the suggestion of a decrease in slope with increasing Au.

The Co–Au (Fig. 1e) and Ni–Au (Fig. 1f) plots show positive, low slopes (and thus limited ranges, factors of ∼1.2) and, at Au >0.9 μg/g, a complementarity in scatter reflecting variations in the taenite/kamacite ratio. At low temperatures the taenite/kamacite concentration ratio for Co is ∼0.2 whereas that for Ni is ∼8 (e.g., Afiattalab and Wasson, 1980). Comparison of the four IIAB irons having Au contents >1.2 μg/g in Figs. 1e and f makes this effect clear. The complementary scatter can be assigned to stochastic sampling of rare taenite in these low-Ni irons.

The six scatter diagrams in Fig. 2 all show negative element–Au trends. Generally this is an indication that the

element is compatible in the crystallizing metal phase. The total range for Cu (Fig. 2a) is small, a factor <1.6. In the four irons with Au > 1.2 μg/g Cu contents show the same variations as Ni, implying similar taenite/kamacite concentration ratios ≫1. The negative trend in Cr is similar to that observed in other groups. Because the Cr D value is <1 at all S concentrations (Jones and Malvin, 1990), the trend should be positive if controlled by metal crystallization; the negative trend could indicate that a trace Cr-rich phase such as chromite is on the liquidus (Ulff-Møller, 1998) or could be related to selection effects introduced by the analyst (Wasson et al., 1999) or both.

The elements W (Fig. 2c) and Pt (Fig. 2d) show very similar, well-defined trends on element–Au diagrams. Total
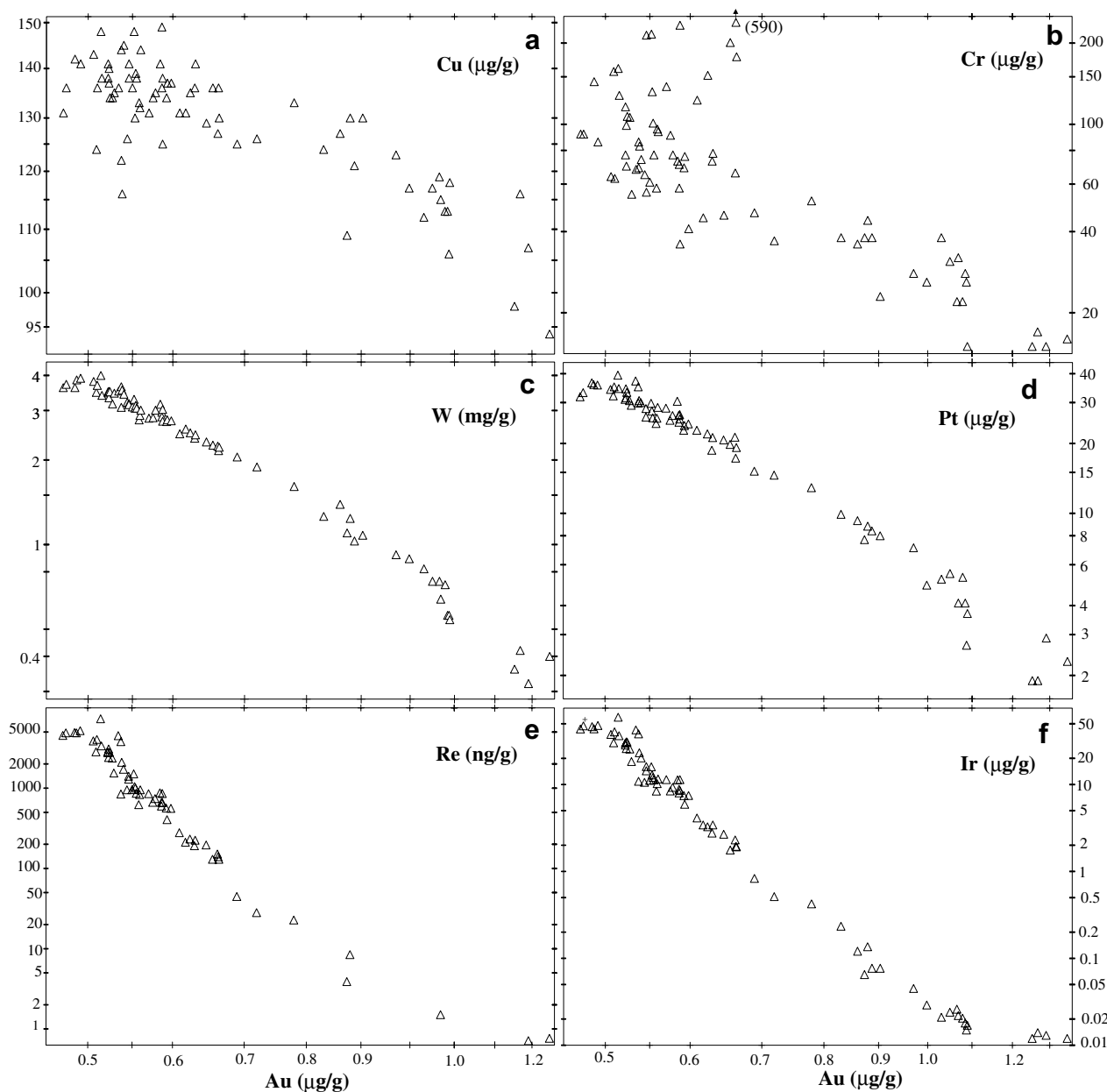
Fig. 2. Log-element, log-Au diagrams for six elements (Cu, Cr, W, Pt, Re, and Ir) showing negative trends indicating compatibility during crystallization of the IIAB magma. The compatibility of Cr is probably with chromite, which may have been on the liquidus during crystallization; exceptionally high contents of Cr-bearing inclusions such as daubreelite are found in the FeS inclusions of some evolved IIAB irons.

ranges are 14–20; uncertainties are relatively large for the 4–5 lowest values. The small spread and the slight downturn at the high-Au end of the nearly linear W–Au array suggested that it could be fit with equilibrium solids with minimal trapped melt effects. Below we examine this possibility in more detail and show that there is evidence for melt trapping.

The final two element–Au diagrams in Fig. 2 show Re (Fig. 2e) and Ir (Fig. 2f). In magmatic groups the ranges of Re and Ir (and Os, not reported) are always large and similar. Because we cannot reliably determine Re below about 20 ng/g, we have incorporated the thermal-ionization mass spectrometry data for 12 IIAB irons studied by Cook et al. (2004) into Fig. 2e and Table 1. The combined

Re data yield a range of 6000, moderately larger than the Ir range of 4000. The slope of both distributions decreases in the high-Au tail. As discussed in detail below, this change in slope reflects the large amount of trapped melt in the IIAB irons having the highest Au contents.

4. Fractional crystallization of the IIAB magma: nonmetal concentrations

4.1. Estimating the concentrations of nonmetals, especially S

There are three large, "magmatic" iron meteorite groups that show large ranges in Ir and negative correlations

between Ir and Au, As and Ni on log-log diagrams. It is now accepted that the large Ir ranges reflect formation by efficient fractional crystallization. Fractional crystallization requires complete mixing of the liquid phase on a time scale very short compared to the total crystallization period. In contrast, the nonmagmatic groups such as the IAB main-group (Wasson and Kallemeyn, 2002) show relatively small Ir fractionations, an indication that the liquid chilled quickly. Rapid solidification is also indicated by the common presence of chondritic silicates trapped in the metal.

As shown by Scott (1972) the more or less linear arrays that the members of magmatic groups form on log-log diagrams are consistent with formation by fractional crystallization in which the solid/liquid elemental distribution coefficients (the "D values") remain constant throughout the crystallization sequence. However, realistic studies (e.g., Jones and Drake, 1983) in which the common nonmetals S, P, and C were included in the system showed that D values depend on the concentrations of these elements in the magma. Because most magmatic irons had low concentrations of C and, until recently (Chabot et al., 2006) there were relatively few laboratory studies of its influence on D values, its effect is generally not modeled. It is, however, of interest that Buchwald (1975, p. 485) observed carbides in Coahuila and 7 other IIAB irons. The concentration of Ni also influences the D values, but to a lesser extent than the nonmetals. Its effect is also not included in the simulations.

Neither S nor P is efficiently incorporated into crystallizing metallic iron. As noted in the introduction, we commonly assume that D_S is 0.005. We generally assume that D_P is 0.1. Even with this higher D value, a very large fraction of the P remains in the melt throughout fractional crystallization. As an example, after 50% crystallization with $D_P = 0.10$, the P content has increased by a factor of 1.87. The S content increases by a factor of 1.99 in the same range.

The nonmetal content of the initial magmas has been estimated in two different ways. Jones and Drake (1983), Haack and Scott (1993) and Chabot (2004) plotted the laboratory D values against the S concentrations on log-log diagrams and represented the trends by linear functions. They then calculated solid crystallization trajectories for different S contents, and selected the S content that yielded the best approximation of the element–Ni or (in Chabot, 2004) element–Au trends through the groups. The key elements in their tests were Ge, Au, and Ir. Chabot and Jones (2003) noted that P and S affected D values similarly and, for convenience, they used the same algorithm relating D values to the concentrations of these elements. Thus, the S values inferred from the Chabot (2004) trend fittings in fact represent the sum of S and P. Chabot (2004) estimated the IIIAB initial S content to be 120 mg/g and the IIAB S concentration to be 170 mg/g, nearly the same as those Haack and Scott (1993) had obtained by a similar method.

Esbensen et al. (1982) and Wasson (1969) took a very different approach to estimating the initial S content. They argued that the wide (factor of 2) range in Ir and Au and

the still larger (factor of 9.7) in S observed among the various large (1–35-ton) masses of Cape York reflected different degrees of melt trapping. Wasson (1999) constructed solid and liquid crystallization tracks on log Ir–log Au and log Ir–log As diagrams, and showed that the compositions could be fit if Cape York-Savik contained about ∼5% trapped melt and Cape York-Agpalilik contained about ∼50% trapped melt. The crystallization trends also indicated that the suite of Cape York irons formed after 30% of the core had crystallized. From these data and the modally determined S content of Cape York-Agpalilik of 13.5 mg/g Wasson (1999) estimated an initial S content of 20 mg/g, 6× lower than that estimated by Chabot (2004). Wasson (1999) compiled modal estimates of S contents for several large IIIAB sections and showed that S contents correlated with the amount of trapped melt inferred from the locus of the composition of the irons on Ir–Au and Ir–As diagrams. Wasson and Richardson (2001) increased the estimated S content of IIIAB to 24 mg/g.

Neither of these methods of estimating initial S is very precise. Estimates based on the relationship between laboratory D values and the S contents of the melt are based on fits to laboratory data that show considerable scatter and that were obtained by techniques having technical challenges (including gravity segregation and the inability to quench the melt to a "glass"). There is no theoretical understanding of how D values should depend on the S and/or P content of the metallic liquid, thus the linear fits on log-log diagrams used by Chabot and Jones (2003) may be forced through trends that are more complex (e.g., not linear on a log-log plot) but not recognizable given the limitations of the data sets.

The method used by Esbensen et al. (1982) and Wasson (1999) could yield low S estimates some of the almost fully crystallized (S-rich) trapped liquid leaked out (perhaps returning to the main magma) of the system during the extended period of crystallization that finally terminates when the eutectic liquid crystallized at about 1290 K, several hundred degrees below the liquidus temperature at which the earliest associated solids formed.

In summary, there is general agreement among researchers that contents of volatile elements including P and S in the IIAB initial magma were appreciably higher than those in the IIIAB magma. This is partly because IIAB Ga and Ge concentrations are 3–5× higher than those in IIIAB irons, and partly because IIAB log Ir-log Ni and log Ir–log Au trends have much higher negative slopes than in IIIAB, implying higher IIAB D values for all three elements. Unfortunately, this agreement on relative values between these two large groups helps to only a limited degree to constrain the actual S and P contents.

4.2. Estimating the P/S ratio in the IIAB magma

Listed in Table 3 are P and S contents in IIAB irons estimated for relatively large (>200 cm^2) IIAB sections by Buchwald (1975) and (generally by modal analysis of

photos) by us. Unfortunately, in most cases Buchwald (1975) failed to note the areas of the sections he integrated. Because Buchwald carried out most of his modal integrations at the Smithsonian Institution in Washington, DC, we assumed that the total area of the large sections present there provide reasonable estimates of the areas studied although in some cases the actual areas will have been larger because sections from other museums were also counted. In one key case, Ainsworth, it appears that his S value represents only one smallish (120 cm^2) section.

With the exception of 12 mg/g in the large mass of Santa Luzia, the highest S content listed in Table 3 is only 3 mg/g, much less than the highest values (21.7 mg/g) reached in IIIAB (Wasson, 1999). As discussed later, this may reflect the presence of immiscible S-rich and P-rich layers in the IIAB core.

In most of the samples studied by Buchwald (1975) the P content is higher than the S content. For those samples having relatively low-S contents and thus low trapped melt-fractions it seems probable that much of the P exsolved from the crystallizing metal, and that the P/S ratio in the IIAB magma was appreciably less than unity. We will use 0.25 g/g as our working assumption of the ratio in the initial IIAB magma, similar to the P/S ratio employed by Wasson (1999) as his working estimate for the IIIAB magma.

The best estimates of the P/S ratio in the magma are obtained from the modal analysis of irons with very high contents of trapped melt. In such cases almost all the P observed in the sample was introduced with the melt. For example, if we assume a high D_P value of 0.15 and a trapped melt content of 300 mg/g, then simple algebra shows that 74% of the total P came with the trapped melt. If the D_P values was 0.1, 81% of the P is attributable to trapped melt.

It is important to note that the P/S ratio in typical chondrites is much lower than those we have estimated for most iron meteorite magmas. The data compilation of Wasson and Kallemeyn (1988) shows that P/S ratios in bulk chondrites range from 0.03 to 0.05 g/g if the value of 0.017 in CI chondrites is neglected. The fact that the ratio in iron meteorite cores is 5–8 times larger requires that most of the chondritic S not have been incorporated into the iron meteorite parental magmas. The two possible loss mechanisms are oxidation or, more likely, volatilization. We suggest that moderate amounts of S were lost as volatile gases at the time of core formation.

4.3. Trapped melt in Santa Luzia and other high-Au IIAB irons

There is abundant evidence of trapped melt in high-Au IIAB irons. As stated above, it is widely accepted that all FeS nodules larger than several millimeters represent trapped melt. The volume of the trapped melt ranges from about 1.2× the volume of the FeS if the melt had the eutectic composition (315 mg/g S) to larger values for smaller S contents in the trapped melt.

It is also clear that large skeletal schreibersite crystals represent pockets of trapped melt. Examples of such crys-

Table 3
Values of parameters used to calculate the IIAB solid and liquid tracks shown in Figs. 5 and 9

Element	D_0 this work	D_0 Cha/Jo	D_0 IID	β this work	β Cha/Jo	β IID
As	0.248	0.22	0.196	1.82	2.2	2.0
Ir	4.15	1.5	1.81	4.6	4.9	4.6
Au	0.335	0.25	0.265	1.4	2.0	2.3
W	1.70	1.2		3.78	3.6	

Parameters recommended by Chabot and Jones (2003) and used by Wasson and Huber (2006) for the low-S magmatic group IID are shown for comparison.

Table 4
Analyses of metal, schreibersite and troilite from a Santa Luzia bar removed from USNM specimen 1618

Sample	Cr	Co	Ni	Cu	Ga	As	W	Ir	Au
A1	12	5.01	60.5	112	46.3	12.1	0.37	0.011	1.345
A2	13	5.17	57.7	106	45.6	12.1	0.41	0.014	1.343
A3	12	5.42	49.9	103	44.0	11.9	0.42	0.012	1.288
A4 (Schreibersite)	19	2.27	159.9	72		1.90	0.29	0.0040	0.0039
A5[a]	10	5.15	57.5	78	39.2	11.0	0.33	0.012	1.116
A6	13	5.17	56.8	92	40.0	11.1	0.54	0.016	1.134
A7	14	4.91	68.0	82	35.4	10.0	0.32	0.012	1.006
A8[a]	12	4.92	62.1	84	36.8	10.4	0.35	0.012	1.091
A9[a]	11	5.17	52.0	100	43.9	11.8	0.39	0.011	1.292
A10	13	4.94	56.3	103	44.7	11.8	0.33	0.012	1.319
A11	12	5.00	63.5	114	46.6	12.1	0.41	0.018	1.382
A12 (troilite)	4060	0.65	34.4	392					0.020

[a] (Some) Schreibersite removed by drilling from these samples.

tals are shown in a section of Santa Luzia (Fig. 3a). In Fig. 3b a sketch modified from one in Clarke and Goldstein (1978) shows that the larger skeletal schreibersite near the center of the specimen surrounds a large troilite inclusion, but that no troilite is associated with the smaller skeletal schreibersite on the left. From the shaded areas we estimate that, in this small (75 cm²) section the P concentration is 6.1 mg/g and the S concentration is 4.8 mg/g. Note that both inclusions are surrounded by large regions of swathing kamacite.

Buchwald (1975) described these inclusions and surrounding kamacite as "schreibersite-metal-troilite eutectics" and estimated that these cover ~30% of the available sections of Santa Luzia. We see no direct evidence that these melts were already eutectoidal when they were trapped, and we interpret the volume of the assemblage differently. In our opinion, the swathing kamacite is coarser than the kamacite forming the Widmanstätten pattern because it nucleated earlier. When the
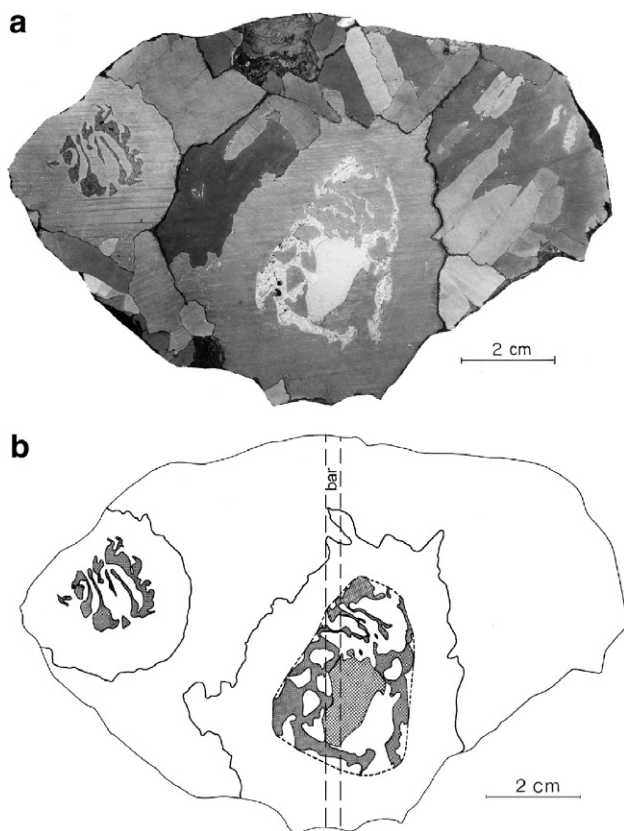
a

b

Fig. 3. Two large regions originally occupied by trapped melt are shown in Santa Luzia specimen USNM 1618. (a) Smithsonian Institution photo of polished and etched section showing the coarsest–octahedrite structure and two skeletal schreibersite inclusions surrounded by swathing kamacite (Smithsonian Institution photo); (b) sketch modified after one in Clarke and Goldstein (1978) showing that the left inclusion consists entirely of schreibersite (fine shading) whereas the central inclusion has schreibersite on the exterior and troilite (grid pattern) occupying the center. Regions that are not shaded in the sketch are kamacite with, at most, traces of taenite; the outer limits of the swathing kamacite around the inclusions are outlined.

assemblage cooled across the boundary between the γ (fcc taenite) and α + γ, the first kamacite (bcc) nucleated on the schreibersite. Because it got a head start, it initially incorporated all the Fe that was exsolving from the taenite as cooling gradually increased its equilibrium Ni. Thus the relative volume of the swathing kamacite regions only offers a rough approximation of the maximum fraction of trapped melt.

The minimum fraction of trapped melt is given by envelopes consisting of smooth curves surrounding the schreibersite and convex towards the swathing kamacite; we illustrate such an outline around the schreibersite in the large inclusion in Fig. 3b. We suggest that these represent the size of the melt-filled pockets at the time the schreibersite began to crystallize on the solid–liquid interface. If, as is probable, schreibersite was not yet a liquidus phase at the time the melt was trapped, the original melt fraction would have been somewhat larger.

If we assume that most trapped melt regions were spheroidal, the fact that some skeletal schreibersite inclusions are associated with troilite and some not can be explained as follows. One observes troilite when the plane of the section passed near the center of the large trapped melt region. If the section did not pass near the center of the region no troilite would be associated with the massive skeletal schreibersite. More complex geometries (e.g., cigar-shaped) would lead to a greater tendency for the late FeS-rich liquid to separate from schreibersite.

Thanks to Dr. Elisabeth Zuccolotto, we have obtained a spectacular image of the large (90 × 25-cm) section of the 1.9-ton Santa Luzia on display at the Museum Nacional in Rio de Janeiro (Fig. 4). This image, made with the face wet with etch solution, allows both troilite and schreibersite to be resolved in most regions. The troilite forms elongated stringers oriented roughly parallel to each other (and to the long dimension of the section). The skeletal schreibersite occupies irregular volumes to either side of the troilite stringers. This image demonstrates that the cavities filled with trapped melt were quite irregular, and more nearly cylindrical than spheroidal. As listed in Table 2, our modal data show that the mean P and S contents of this region of Santa Luzia are 6.6 and 12.3 mg/g, respectively; because the surface area is large, these should be representative for this large mass. Note the large discrepancy between the S estimates for the large specimen and the small specimen shown in Fig. 3a.

Because we do not know the mechanical mechanism that led to melt trapping we cannot be sure that a late, FeS-rich melt could not have escaped. It nonetheless seems more plausible that the inclusions in Santa Luzia are representative, in which case one concludes that the P/S ratio in the trapped melt was ~0.54, appreciably higher than the value of 0.25 g/g we assumed for the initial composition of the IIAB magma. We will return to this point below in our discussion of immiscible metallic melts.

Fig. 4. Large (50 × 180-cm) polished section of Santa Luzia on display at the Museum Nacional in Rio de Janeiro; the specimen was photographed while wet with etch solution. The troilite (bronze) forms elongated nodules roughly aligned with the long axis of the section. Schreibersite forms skeletal inclusions in the metal on either side of the troilites; a minor fraction of the schreibersite is in direct contact with the troilite. Modal integration yields 4.7 vol% schreibersite and 5.5 vol% troilite on this surface.

4.4. Estimating the liquidus temperature of the initial IIAB magma

The liquidus temperature of the IIAB parental magma is mainly controlled by the assumed nonmetal concentrations; 60 mg/g S and 15 mg/g P. From the binary phase diagrams in Brandes and Brook (1998) we estimate a liquidus temperature for 75 mg/g S (remainder Fe) of 1675 K and a liquidus temperature for 75 mg/g P (remainder Fe) of 1498 K. Thus, if the P/S ratio was 0.25, interpolation yields a liquidus temperature of 1630 K. Replacing some Fe with about 60 mg/g Ni would surely lower this further, perhaps by about 10 K. Thus a rough estimate of the liquidus temperature is 1620 K. Our later discussion of liquid immiscibility suggests a higher initial liquidus temperature, perhaps ∼1635 K. The actual initial value is probably somewhere in the range 1625–1635 K.

5. Fractional crystallization: Modeling Ir–Au and Ir–As trends

In Fig. 5 we illustrate solid and liquid tracks modeled to fit the IIAB data. We used the Chabot and Jones (2003) algorithm (Eq. (1), obtained by taking the logarithm of their Eq. (8) after dropping the carbon terms) relating the logarithms of the D values to nonmetal contents but we adjusted the two constants (D_0 and β) to maximize the fit to the IIAB iron meteorite trends.

$$\log D = \log D_0 - \beta \cdot \log\left[(1 - 2X_S - 3X_P)/(1 - X_S - X_P)\right]. \quad (1)$$

We carry out the fitting process by trial-and-error and thus cannot claim that we have arrived at a unique solution. The shapes of the solid and liquid tracks on Fig. 5 are good approximations of those needed to explain the IIAB scatter field but similar shapes can be achieved with modestly dif-
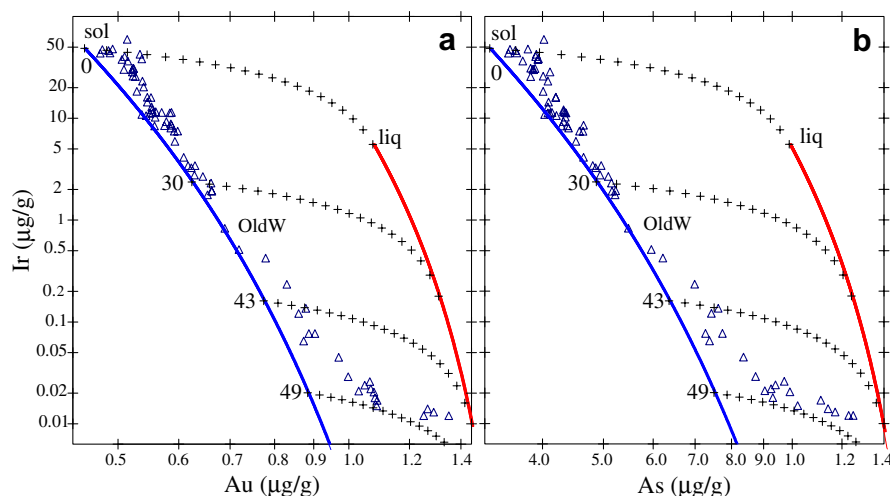

Fig. 5. Log–log plots of Ir vs. (a) Au and (b) As for IIAB irons. Estimated solid and liquid tracks are shown; IIAB data for high-Ir irons plot near the solid track. Solid–liquid mixing curves are shown at 0, 30, 43, and 49% crystallization; the distances between adjacent crosses correspond to 5% differences in the inferred amounts of trapped melt. For irons with >0.05 μg/g Ir the maximum inferred amount of trapped melt is 13% (in Guadalupe y Calvo). At lower Ir contents the inferred fractions of trapped melt range from roughly 15% in Iredell to 70% in Santa Luzia. Note that the position of Santa Luzia constrains the D_{Au} and D_{As} values to be relatively low, about 0.6 g/g. The point with the highest Ir value, Avce, is believed to contain an unrepresentatively high fraction of taenite.

ferent sets of constants and nonmetal concentrations within the Chabot–Jones parameterization. In addition, we suspect that this parameterization is only an approximation of the chemical physics of the actual magmas. We suggest that significant progress in understanding the chemical physics will be necessary before one can proceed further but that, in the interim, the best approach is to construct plausible solid and liquid tracks that modelers can attempt to match.

We will therefore provide more detail about the goals, assumptions and the model-dependent "constraints" involved in arriving at the "fits" shown in Fig. 5. The first assumption is that the first crystallized solids are represented in our set of IIAB irons. This appears to be a reasonable assumption in all the large magmatic groups. If this assumption is correct, the initial liquid gives the bulk composition of the entire core.

The second assumption is that the left envelope of the distribution corresponds approximately to the track of solid compositions produced by the fractional crystallization process. Because all IIAB irons contain FeS nodules it is clear that some trapped melt is present. If, as we assume, the initial S content of the IIAB magma was 60 mg/g, the FeS contents tabulated in Table 2 suggest that most IIAB irons contained 1–3% trapped melt. We therefore chose Au and As contents in the initial liquid about 1% lower than would yield a best fit of the irons that plot closest to the left envelope. We did not adjust Ir; for low degrees of trapped melt the Ir analytical uncertainties contribute more to the uncertainty in the choice of the Ir content of the initial liquid than do the uncertainties in the amount of trapped liquid.

The third assumption is that (with rare exceptions) the melt that is trapped was in equilibrium with the surrounding solids at the moment it was trapped. The end-member alternative is that early solids became mixed with a late melt. Intrusion of a late melt has almost certainly occurred for the IIIAB irons Treysa, Delegate and Tieraco Creek (Scott, 1977; Wasson, 1999) and seems to have been common in the main-group pallasites (Wasson and Choi, 2003). Because trapping equilibrium melt is a simpler process that is adequate to explain most of the iron meteorite data trends we use it as our default model. We therefore show equilibrium mixing curves on our diagrams. A corollary of the third assumption is that, where large areas can be integrated to obtain modal estimates of the amount of FeS, the amount of trapped melt inferred from the position on an Ir–Au or Ir–As diagram will roughly correlate with the FeS content.

In Fig. 6 we test this corollary. Because D_S is ~0, the concentration of S in the magma is expected to increase in proportion to 1/(1-G) where G is the degree of crystallization. We therefore multiplied the modally estimated S contents from Table 2 times (1-G) estimated from our modeling shown in Fig. 5 and plotted this product versus our estimates of the fraction of trapped melt. The data form a cluster of points having low corrected S contents and low trapped-melt fractions and Santa Luzia, with high
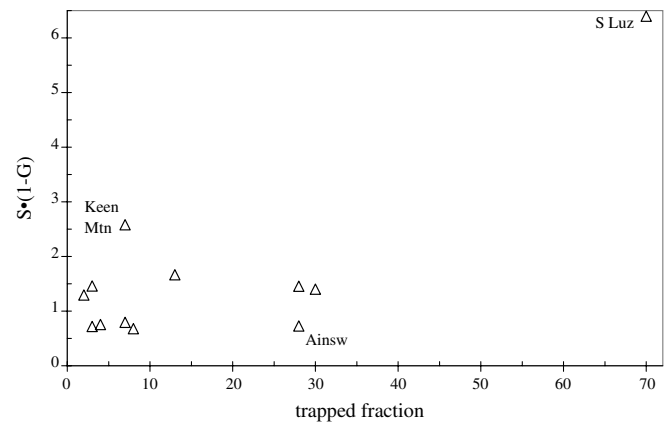

Fig. 6. Corrected S content is plotted against trapped melt-fraction read off the Fig. 5 diagrams. This diagram tests the prediction that these two measures of trapped melt should be positively correlated. Because S is essentially not incorporated into the metal, the S content must be corrected for the degree of crystallization of the magma; it is therefore multiplied by (1-G). A positive trend is observed, dominated by the Santa Luzia value in the upper right. The model S contents of the two most deviant irons, Keen Mountain and Ainsworth, are based on the integration of relatively small sections.

values of both. We label Keen Mountain and Ainsworth, the two points showing the greatest deviation from a smooth trend. Table 2 shows that these values (from Buchwald, 1975) are based on small areas, <230 cm², and thus are subject to high sampling errors. We conclude that the diagram is consistent with our corollary, but that confirmation will require the study of appreciably larger sections of the IIAB irons.

The third assumption and its corollary lead to the conclusion that we can use samples with high-FeS contents to roughly constrain the D_{Au} and D_{As} values applicable at the degree of crystallization at which the melt was trapped. For example, the highest modal FeS contents in IIAB are in Santa Luzia and Sao Juliao. We account for these by mixes of about 30% solids and 70% trapped melt occurring after slightly more than 48% of the magma had crystallized (Fig. 5). In our preferred model we used $D_{Au} = 0.53$ and $D_{As} = 0.46$. If these D values were >20% larger the liquid track would pass on the left side of them and their positions would be inconsistent with formation by equilibrium melt trapping.

To illustrate the interplay of the various parameters that we adjust by our trial-and-error manipulations consider the following. Had we felt that 70% trapped melt was too large a fraction, the apparent solution would be to reduce the values of D_{Au} and D_{As} in order to increase the distance between the solid and liquid tracks. We would, however, want to leave the position of the solid track close to the position shown on Fig. 5. The D_{Ir} value that corresponds to the D_{Au} value of 0.53 at 48% crystallization is 23. Suppose that we felt that the amount of trapped melt was more likely to be ~40% and that we should therefore force the D_{Au} value to be about 0.4. To obtain the same slope for

the solid track we would now need to make the D_{Ir} value be 33; decreasing D_{Au} thus requires a major increase in D_{Ir}. The published experimental estimates of D values show that this combination is less plausible than our values which produced the estimate of 70% trapped melt (Fig. 5).

In Table 3 our preferred parameters are compared with the "universal" parameters of Chabot and Jones (2003) and with those used in our recent paper discussing the low-S group IID. In Fig. 7 we show the solid and liquid Ir–Au and Ir–As tracks produced by the Chabot–Jones parameters and by the Chabot (2004) preferred "S" content of 170 mg/g (although we actually used 136 mg/g S and 34 mg/g P in our simulation, Chabot states that she feels that the observed low-S contents in IIAB would suggest 160 mg/g S and only 10 mg/g P). The calculated solid track provides an excellent fit to the left envelope of the IIAB scatter field at Au concentrations <0.75 μg/g. However, the most striking feature of the diagram is that, although the initial liquid is slightly above the solid track, it immediately plunges vertically across the solid track and achieves a positive trend (because D_{Au} and D_{As} have increased to values >1). This model leaves about half of the IIAB irons stranded in no man's land; they cannot be explained by any mixture of solid and liquid, equilibrium or nonequilibrium. Because this model does not explain these irons, it casts serious doubt on this method of estimating the S contents of iron meteorite groups.

Additional evidence against the model is based on liquid immiscibility discussed later in the paper. Because the Chabot initial composition is within the two-immiscible-liquid stability field, tielines similar to those suggested by Ulff-Møller (1998) indicate that the initial P-rich liquid would contain 58 mg/g P and 21.5 mg/g S, a P/S ratio of ~2.7. The absence of massive schreibersite associated with FeS
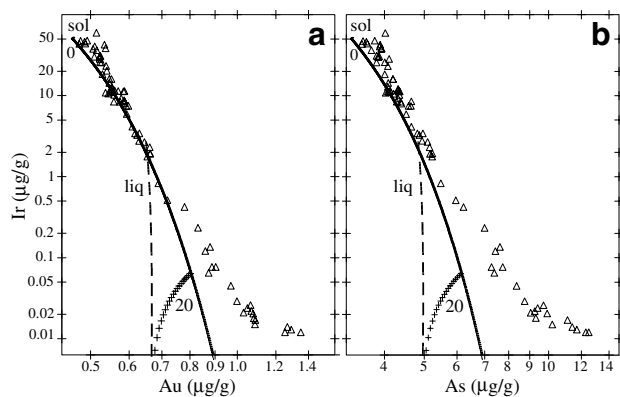

Fig. 7. Log-log plots of Ir vs. (a) Au and (b) As for IIAB irons. Solid and liquid tracks calculated using a combined S and P content of 170 mg/g recommended by Chabot (2004) and the Chabot–Jones (2003) constants (see Table 3) are shown The solid track provides a good fit to the left envelope of the IIAB distribution, but the liquid track plunges vertically at Au ~0.67 and As ~5. An equilibrium mixing curve at 20% magma crystallization is shown. This model cannot explain the irons have Au contents >0.8 μg/g, all of which plot to the right of the solid track. Neither equilibrium nor nonequilibrium mixing can produce compositions in this part of the diagram.

nodules in low-Au IIAB irons indicates that the P/S ratio was much lower, surely <1 and probably near 0.25.

Comparison of the Wasson and Huber (2006) IID parameters with those we use for IIAB shows significant differences that require discussion. The β values for Ir are identical and those for As are essentially the same. Those for Au are appreciably different but, because the S content was quite low in the IID magma, we could have used a β value as low as 1.6 without impacting the model in a major way. In contrast, the models are quite sensitive to the intercept (the D_0 values), and we found that our IIAB model required much higher values for these than did the IID model. We had also found a similar pattern in earlier studies. For group IIIAB, which has a high mean S content and a high negative slope on Ir–Au and Ir–As diagrams, Wasson (1999) chose a high D_0 value (4.6) for Ir. In contrast, for group IVA Wasson et al. (2006) chose a D_0 value of 1.62. Thus, there is a general trend in our fitting models that, the higher the initial S content, the higher the intercepts that yield the best fits to the trends. It should be noted that these are fitting parameters corresponding to one segment of the trend in Ir–Au and Ir–As space; there is no requirement that the intercepts correspond to the actual D_0 values measured at low nonmetal concentrations.

Although application of Occam's razor suggests that this discrepancy should lead to skepticism about our model, we argue that our model fits will prove to be better when the chemistry and physics of these metallic liquids are better understood. We suggest that there are different regimes within metallic liquids, and that the overall trend in the relationship between D and the nonmetal contents changes as one moves from (1) metallic systems in which the nonmetals play relatively minor roles to (2) intermediate systems in which an appreciable fraction of the first and second nearest neighbors of Fe or any other siderophile are nonmetals to (3) sulfidic systems in which the mole fraction of FeS is greater that the mole fraction of the remaining Fe (and Ni). Note that, in an equal molar mix of Fe and FeS the atomic fraction of S is 33.3% and the mass fraction is 22.3%. A possible explanation of the large shift in the Ir D_0 values is that there is an abrupt transition between regimes 1 and 2. We suggest that we are fitting short segments of the overall trends with our trial-and-error techniques and that the Chabot–Jones (2003) algorithm is the result of forcing a linear fit through a more complex relationship with the actual trends hidden in the scatter.

The data for group IVA provide evidence in support of this viewpoint. In Fig. 8 we plot the IVA data on Ir–Au and Ir–As diagrams. These diagrams are edited versions of those in Fig. 8 of Wasson et al. (2006), the difference being that we have merged the silica-bearing IVA irons into the main data set. The negative trends formed by the left envelope of the data are shallow up to Au ~ 1.6 μg/g, and much steeper thereafter; the same abrupt change in slope occurs at As ~ 8.5 μg/g. We suggest that this large change reflects the transition between melt regimes 1 and
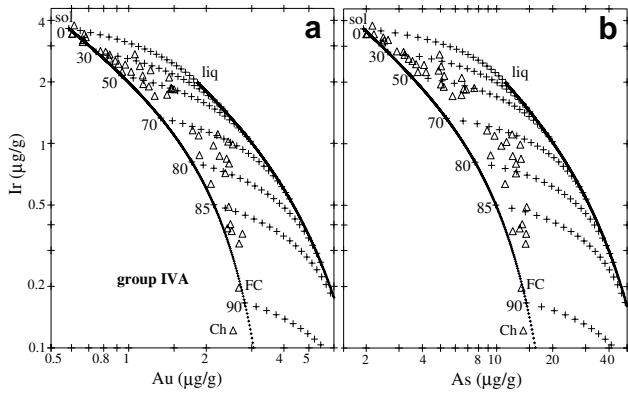
Fig. 8. On log-Ir, log-Au and log-Ir, log-As plots of IVA iron data the irons forming the left envelope (i.e., those with low contents of trapped melt) show a low slope up to Au = 1.6, As = 8.5, but a much steeper slope for the irons having higher concentrations. We suggest that this indicates that the magma evolved through two different liquid regimes, with nonmetals playing a minor role in the first but a pronounced role in the more evolved magma. This is an edited version of Fig. 8 of Wasson et al. (2006); the choice of parameters used for the solid and liquid tracks (which were not intended to account for differences in liquid regimes) can be found there.
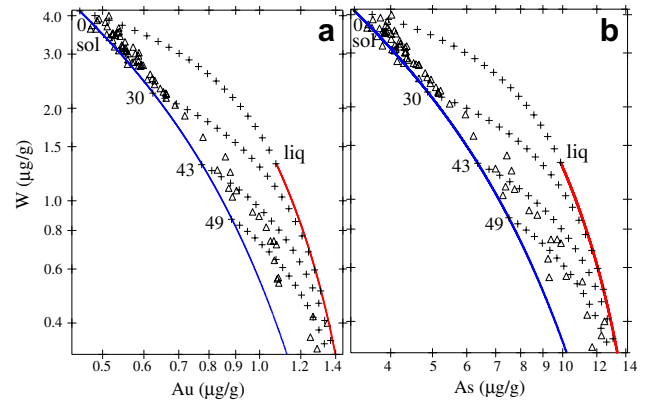

Fig. 9. Log-log plots of W vs. (a) Au and (b) As for IIAB irons. The W–Au (Fig. 2e) and Pt–Au (Fig. 2d) diagrams showed downward trends at high-Au values suggesting that they did not show the influence of trapped melt. Here we plot the W data (which has higher precision than Pt) against Au and As. The set of high-Au irons that show evidence of trapped melt in Fig. 5 shows the same trends on W–Au and W–As diagrams. Because of high errors in W concentrations <0.4 μg/g the apparent trapped-melt fractions have high uncertainties.

2, and that the increase in D_0 occurred over a relatively small range of S concentrations.

We mentioned in connection with Fig. 2c that the W–Au trend (and the less-well-defined Pt–Au trend in Fig. 2d) seemed to disagree with predictions of the trapped melt model. We therefore carried out a detailed modeling of W–Au and W–As trends; the result is shown in Fig. 9. In fact, the patterns are much the same as the Ir–Au and Ir–As trends and evolutionary tracks illustrated in Fig. 5 even though the factor of 11 W range is much smaller than the factor of 4000 Ir range. At Au values up to 0.7 μg/g the data plot close to the solid track; at higher Au values the points scatter in the direction of the liquid track. Although the two sets of diagrams differ in details, we attribute most of the differences to the much higher uncertainties in W compared to Ir.

6. Evidence of trapped melt and liquid immiscibility in group IIAB

As discussed in various papers, most recently by Chabot (2004), group IIAB is inferred to have had an exceptionally high initial S content. Part of the evidence is the generally high volatile (e.g., Ga and Ge) contents of IIAB irons. Equally important are the steep negative slopes on Ir–Au or related diagrams and the very high contents of troilite and schreibersite present in some of the high-Au members of IIAB.

As noted by Ulff-Møller (1998) the increase in the S and P contents resulting from fractional crystallization of iron meteorite magmas can lead to the formation of immiscible S-rich and P-rich fluids. The immiscibility field grows with increasing S and P content of the magma and with decreasing temperature. The Fe–P–S system was studied by

Schürmann and Neubert (1980) and reviewed by Raghavan (1988). The highest temperature at which immiscible magmas can coexist with metallic Fe is 1550 K. Immiscible-liquids can still form at superliquidus temperatures.

In Fig. 10 we show some boundaries copied from Fig. 2 in Schürmann and Neubert (1980). The continuous curve crossing the diagram from upper left to lower right shows the projection of the two-liquid liquidus on the Fe-rich corner of the S–P–Fe diagram. The diamond shows the point at which the S-rich and P-rich liquids have the same composition; this is a critical point; at higher temperatures solid metal cannot exist in equilibrium with two liquids. Three tie lines are shown; these are calculated following the suggestion of Ulff-Møller (1998) that they all coverage onto a "pivot point" at S = 280 mg/g, P = −5 mg/g. The slope of the tie line is the tangent to the curve at this point. Note the steep negative slope of these tie lines.

[Chabot and Drake (2000) also studied immiscibility in the Fe–S–P system. From an undisclosed number of trials they had five that showed "clear separation of the phases". Two of these agreed with the two-liquid boundary of Schürmann and Neubert (1980) (abbreviated SN1980). The three other pairs had much higher S contents in the P-rich liquid. Based on these results CD2000 proposed a new boundary; we show the part of it most relevant to iron meteorites in Fig. 10.

Clearly one (or both) boundaries is not correct. One difference in the two sets of experiments is that CD2000 included Ni and per cent amounts of other siderophiles in their experiments whereas SN1980 included only Fe, S, and P. Another difference is that SN1980 report isotherm curves for systems containing two liquids but no solid; we suspect that such experiments are more straightforward to carry out than those involving solids. It must be difficult to achieve separation of minor fluid fractions in the presence of a potentially wetable solid.
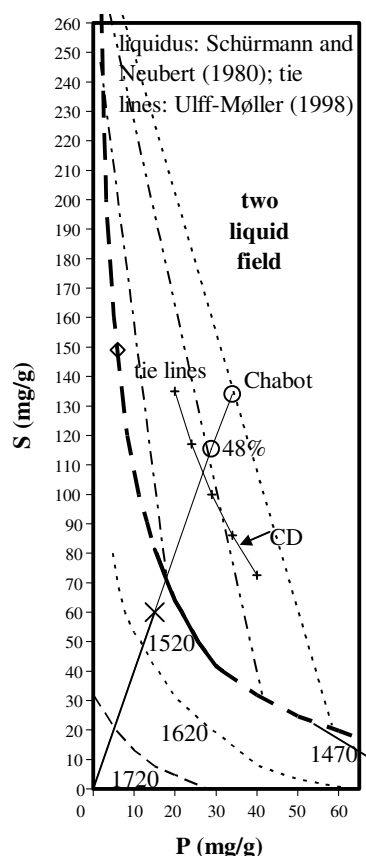
Fig. 10. Projection of the two-liquid surface onto the Fe-rich corner of a Fe–S–P compositional diagram (after Schürmann and Neubert, 1980). The heavy dashed curve shows the boundary of the two phase region; a portion shown solid is particularly relevant to the formation of iron meteorites; it is nearly isothermal at 1520 K. The curves labeled 1720, 1620 and 1470 show the positions of single melts in equilibrium with solid iron at these temperatures. The X shows our assumed initial composition of group IIAB (60 mg/g S, 15 mg/g P); the line passing through it shows the locus of points having the same P/S ratio of 0.25 g/g. The tie lines are calculated using the algorithm of Ulff-Møller (1998). The arc defined by + signs and labeled CD2000 shows a proposed revision by Chabot and Drake (2000). See text for additional details.

Because it appears that many more experiments were carried our by SN1980 (and earlier studies in the same laboratory) than by CD2000, we will use the SN1980 boundary in our discussion. The main conclusions would not be changed if we use the CD2000 boundary].

Some isotherms are shown in the lower left part of the diagram; these mark equilibrium boundaries between the solid and a single liquid . Note that allowance for ca. 60 mg/g Ni would produce temperatures about 10 K lower than those shown. The dark arc labeled 1520 K on the two-liquid boundary shows a portion of the surface relevant to studies of iron meteorite magmas. The temperature is not constant; it falls slightly with decreasing S and increasing P. We assume that the presence of Ni would also cause a ca. 10-K decrease in this boundary.

The X locates the position of our assumed starting composition of 60 mg/g S, 15 mg/g P. A line from the origin passing through this point shows the locus of metal compositions having this typical iron meteorite P/S mass concen-

tration ratio of 0.25. The dotted extension of this line roughly approximates the evolution of the mean liquid composition resulting from the crystallization of metal (it does not make allowance for the fact that P is more soluble than S in solid metal; allowance for this would steepen the trend). The intersection of this line with the two-liquid field occurs at 72 mg/g S and about 18 mg/g P and would be reached after about 20% crystallization of the magma. At this point a tiny amount of S-rich magma (containing ∼240 mg/g S) would separate, and the dominant, P-rich magma would start to increase in P and decrease in S content. The lower circle near the extension of this line shows the composition of our model magma after 48% crystallization (116 mg/g S, 29 mg/g P) corresponding to the most evolved IIAB irons. The upper circle shows the starting IIAB composition (136 mg/g S, 34 mg/g P) inferred by Chabot (2004); the implications of liquid immiscibility occurring at this composition are discussed earlier in the text. Implications of the 48%-crystallization composition are discussed below.

The initial density of the S-rich liquid would have been in the range 4.7–4.9 g cm^{-3} (Nagamori, 1969) and the density would have decreased with continued evolution. The density of the P-rich and Fe-rich liquid would have been much higher, about 7.3–7.5 g cm^{-3}, though its density would also have evolved downward. As noted in Wasson and Huber (2006), the density of chromite (4.8–5.0 g cm^{-3}) is intermediate between these values, this increases the importance of the question raised earlier of whether chromite was a liquidus phase during IIAB crystallization. Even though most of the Cr in IIAB irons is now present as daubreelite (FeCr$_2$S$_4$) we are confident that chromite was more abundant than daubreelite in the chondritic parental materials of group IIAB, and thus that chromite was a liquidus phase throughout crystallization. We do not know of evidence bearing on the issue of whether daubreelite might also have been a liquidus phase, but our sense is that it would be complexed in a S-rich magma and would not exsolve.

Although the S-rich liquid collected at the top of the magma chamber, initially this would have produced no appreciable compositional record in the crystallizing metal. With continued crystallization of metal the relative fraction of the S-rich liquid would increase, the P/S ratio would decrease in the S-rich liquid and increase in the P-rich liquid.

Metal could crystallize both at the top and the bottom of the chamber. However, most crystallization occurred at the bottom of the core. Wasson et al. (2006) argued that, in the low-S IVA core, the thin (nonconvecting) boundary-layer at the lower solid–liquid interface was, on average, much thinner than that at the outer edge of the core, the result of buoyancy effects. They noted that this would have led to a much higher (1–2 orders of magnitude) rate of crystallization at the bottom of the core. In a two-layer core the difference in boundary-layer thickness is likely to have been enhanced, since the viscosity contrast between the upper and lower boundaries was much higher than in the single-layer IVA core.

Initially the volume (and thus the vertical depth) of the upper core was small, and diffusion and convection would have caused it to remain in equilibrium with the crystallizing lower core. Crystallization would have gradually increased the relative volume of the upper core and a key question is whether at some point its thickness would have been too large to allow a close approach to equilibration with the lower core. The deposition of S-rich liquid exsolved from the lower core should still have produced convection. A chromite slurry, if present, would not have prevented the addition of small parcels of S-rich liquid to the base of the S-rich magma. Thus the lowest level of the upper core would have become less dense, and gravitationally unstable.

Fig. 11 is a cartoon showing our picture of the interface region between the upper, high-S and lower, high-P core regions. Kracher and Wasson (1982) noted that convection in a two-layer core does not guarantee that the two-layers will remain in equilibrium. They pointed out that, adjacent to the mutual interface, each layer will have a stagnant layer that is not participating in the convection. If chromite was a liquidus phase (as expected because it was almost certainly present in the parental chondritic materials from which the IIAB magma formed and because chromite formation may explain the negative slopes on Cr–Au and Cr–As diagrams), those grains that did not become attached to metal would have accumulated at the interface between the two cores; this would have both added a physical barrier as well have increased the thickness of the stagnant zone. It is thus possible that, with increasing evolution of the IIAB core, the degree of equilibration between them decreased.
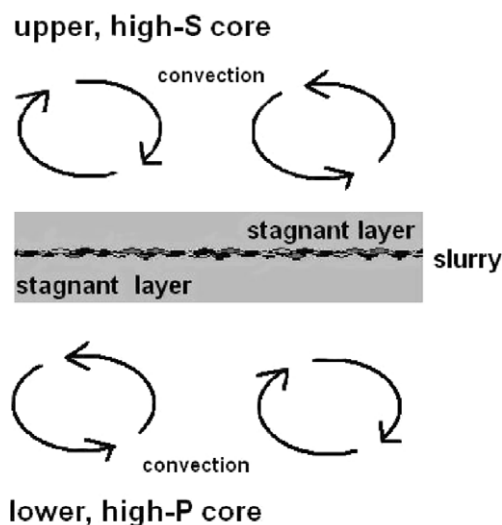

Fig. 11. Cartoon showing the interface region between the high-S upper core and the high-P lower core produced by liquid immiscibility. Both parts of the core would have convected, the lower as a result of the release of latent heat and nonmetal-enriched liquid during crystallization at the bottom of the lower core (where most crystallization occurred), the upper because immiscible S-rich liquid continued to exsolved from the lower core. In the beginning the two cores probably remained in equilibrium, but the stagnant layers and a hypothesized chromite slurry separating them may have eventually reduced the degree of equilibration.

As noted by Ulff-Møller (1998), if equilibration of the two liquids ceased, continued crystallization would gradually lead to a divergence in the composition of the resulting metal. D values would have evolved independently and crystallization trends would produce different patterns. In IIAB, it appears that only a relatively minor amount of crystallization (perhaps 10–15%) occurred after equilibration was no longer approached. We therefore did not expect to see evidence of divergent compositions and none has been recognized.

If irons formed at the top of the core are present in our collections and if they contain large amounts of trapped melt, they should record very low P/S ratios. This ratio provides the definitive test of whether an iron formed in the upper or lower core. At 48%-crystallization the predicted P/S ratio in the upper core is 0.04.

As the volume of the S-rich liquid increased the P/S ratio of the lower core would have increased. We noted above that, in the large section of Santa Luzia the P/S ratio in the large, trapped-melt inclusions is about 0.54, more than twice as high as our assumed initial ratio of 0.25. Because the liquid being trapped was from the lower core, the Santa Luzia observation is not inconsistent with a much lower initial P/S ratio. If we use the P content as a rough measure of the degree of crystallization, then 50% crystallization would produce a P-rich liquid with 30 mg/g P, which the phase boundary indicates to be associated with a S content of ~42 mg/g S, in rough agreement with the estimated Santa Luzia ratio. Although we cannot use this evidence to make a quantitative estimate of the initial P/S ratio, the results are not inconsistent with our assumed value.

Particularly striking is the ubiquitousness of skeletal schreibersite in high-Au IIAB irons. Fig. 12 shows occurrences in three irons with Au >0.9 µg/g. The positions of Ainsworth and Derrick Peak on Fig. 5 imply about 30% trapped melt; as discussed, Sao Juliao is estimated to contain 70% trapped melt. Skeletal schreibersite is rare in the irons plotting close to the solid tracks on Figs. 5a and b; we do not know of any occurrences. Our modal analysis of these images shows that the P content of this small section of Sao Juliao is 12 mg/g. The large Derrick Peak section integration is included in Table 2; it contains 2.6 mg/g S and 3.5 mg/g P.

The descriptions of high-Au IIAB irons given by Buchwald (1975) show that, in most cases, skeletal schreibersite is more common than troilite. Because of the possibility of escape of a late liquid we cannot draw quantitative conclusions, but our inference is that this implies a P/S ratio >0.3 in the associated magma, and that this indicates that they all formed within the P-rich lower-layer of the IIAB core.

7. Attrition of IIAB irons and the missing mass of the IIAB core

Our modeling yields the result that the most evolved IIAB irons represent only 48% crystallization of the parental magma. If one assumes a higher nonmetal content in the
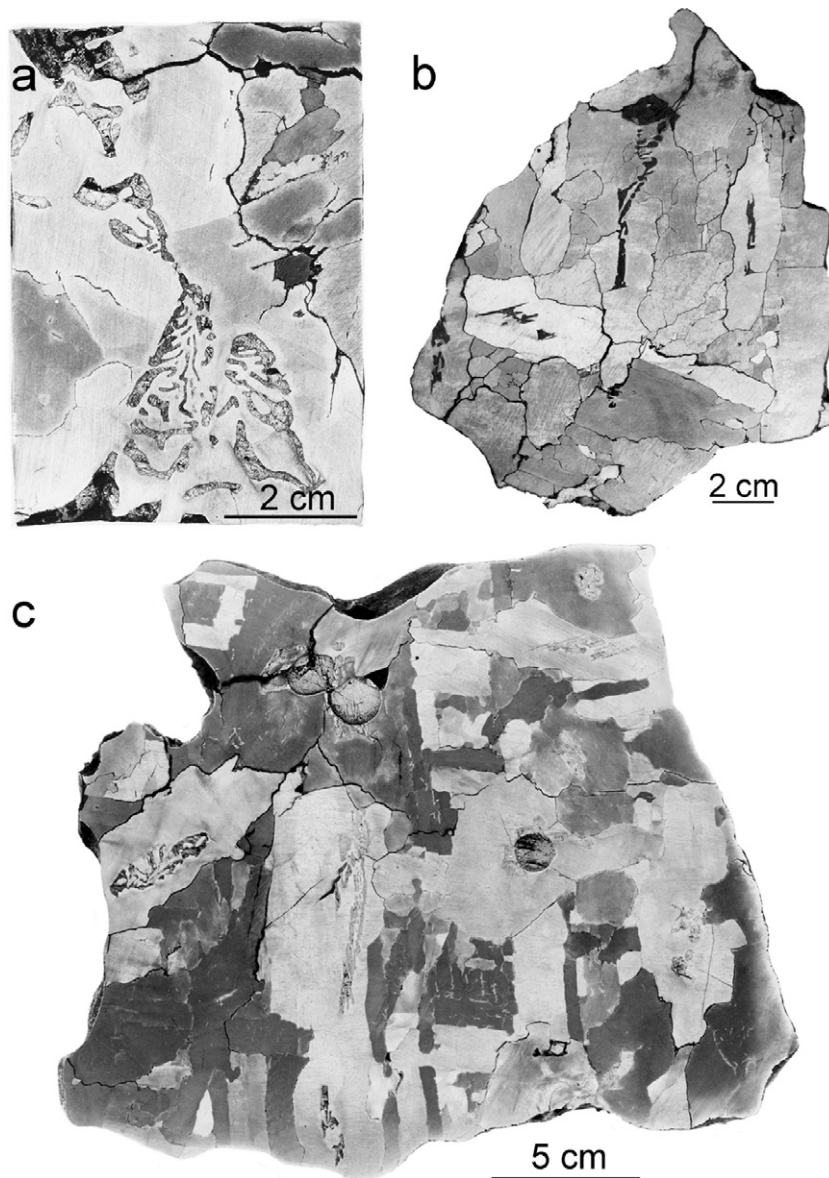
Fig. 12. Photos of three high-Au IIAB members each displaying abundant skeletal schreibersite. (a) Sao Juliao shows beautiful skeletal schreibersite embedded in kamacite; the dark inclusions on the upper and lower left are troilite. (b) The Central Missouri specimen of the Ainsworth shower shows four large regions of skeletal schreibersite set in the centers of the swathing kamacite that nucleated on them. (c) In this large section of Derrick Peak 78008 the troilite forms one circular inclusion and a larger figure-8-shaped inclusion, both sited at kamacite grain boundaries; skeletal schreibersite is located in the interiors of several kamacite patches. Smithsonian Institution photos.

initial magma, the resulting higher D_{Ir} requires that the IIAB range be accounted for by still lower degrees of crystallization. This raises the question of the fate of the missing IIAB materials.

The FeS-rich fraction of asteroids is underrepresented in meteorite collections. The common explanation is that such materials were almost entirely destroyed by erosional processes in space (Kracher and Wasson, 1982). In our opinion, this explanation for the dearth of FeS-rich materials is still the best.

Interestingly, the largest preserved IIAB iron (Santa Luzia, 1.9 tons) has one of the highest contents of FeS and schreibersite. If this mass had entered the Earth's atmo-

sphere at a high-angle, it would surely not have remained intact. We interpret its survival to be fortuitous, the result of a (low-probability) low-entry-angle, low-encounter-velocity trajectory that produced much less stress than a high-angle, high-velocity entry.

Structure matters in the survival of IIAB irons in space and during atmospheric passage. The largest preserved IIAB hexahedrite individual is part of the Coahuila shower. This object, now at Harvard University, has mass of 318 kg and was originally a few percent larger. There are three coarsest-octahedrite IIAB members for which much larger individual masses are preserved: Old Woman (2750 kg), Santa Luzia, Sikhote-Alin (1745 kg) and Navajo

(1500 kg). Sikhote-Alin is the largest observed fall; in addition to the 1.7-ton mass that has a shield shape implying a lift-generating atmospheric orientation a still larger mass created an impact "hole" 26 m in diameter. The largest known IIAB (the coarsest octahedrite Veevers) created a crater 80 m in diameter.

Hexhedrites are generally large (up to at least 40 cm) single crystals of α-iron with a body-centered cubic structure. As noted by Buchwald (1975) and earlier authors, α-iron shows cubic cleavage. He called attention to the fact that museum specimens demonstrate that Braunau and other hexahedrites had been split by hammer and chisel. There are specimens of several hexahedrite falls whose faces correspond to the cubic planes of α-iron.

It has therefore long been argued that the relatively small sizes of hexahedrites reflects their weakness. Collisions in space and stress generated during atmospheric passage have probably reduced the recovered sizes to a greater degree than experienced by the coarsest-octahedrites. Because this process can occur at all sizes, it seems probable that the relative abundance of hexahedritic materials in the IIAB parental core was much higher than observed in the present-day meteorite collections.

8. Summary

The IIAB irons formed by the crystallization of a magma having high contents of S, P, and volatile elements. Evidence for this conclusion are the high observed contents of trapped melt in some irons, the high contents of Ga and Ge, and the fact that trends on log-Ir, log-Au diagrams are steeply negative. Experimental studies show that D_{Ir} and D_{Au} values increase with increasing S and P. The steep slope reflects high D_{Ir} values and D_{Au} values higher than present in other iron meteorite magmas but appreciably lower than unity.

We generated our trial-and-error fits of the IIAB Ir–Au and Ir–As trends using a linear equation of Chabot and Jones (2003) to relate log D value to log metal composition. We found that achieving plausible log D_{Ir} variations require a high intercept (log D_0). In earlier studies we found that group IIIAB (which also has a high nonmetal content) required high intercepts whereas D_0 values for two groups (IID and IVA) with low nonmetal contents were much (2–3×) lower. We suggest that the chemical physics of the metallic melts with low nonmetal contents is very different from that of melts with moderate nonmetal contents, and that dramatic changes between these regimes occur during a relatively small range of nonmetal concentrations. At high nonmetal concentrations D_0 is just a fitting parameter that is not directly related to experimental studies of partitioning at zero nonmetal contents.

As a result of the high-S and -P content of the IIAB magma, after a minor amount of crystallization it began to exsolved a second, high-S, immiscible-liquid. Because the upper and lower core layers approached equilibrium during most of the the subsequent evolution of group

IIAB, metal compositions are not expected to show offsets marking the transition from one-liquid to two-liquid melts. The trapped melt composition observed in IIAB irons such as Santa Luzia that contain large amounts of troilite and schreibersite provide definitive evidence regading the (P-rich or S-rich) nature of the parental magma. Inclusion abundances show that the later-formed IIAB irons all originated in the lower, P-rich core layer.

As discussed by Kracher and Wasson (1982) and others, the absence of evolved, nonmetal-rich meteorites from the IIAB asteroid appears to mainly reflect enhanced attrition of these by impact erosional destruction in space.

Appendix A. Schreibersite, troilite and metal in a Santa Luzia slab and bar

Clarke and Goldstein (1978) used the electron microprobe to study schreibersite and adjacent metal in a large (8 × 13-cm) slab (USNM 1618) of the nonmetal-rich, low-Ir IIAB Santa Luzia. A photo of the slab is shown in Fig. 3a; Fig. 3b is a sketch by Clarke and Goldstein showing the distribution of schreibersite and troilite on the exposed surface. The large schreibersite-troilite assemblage near the center of the slab beautifully illustrates that the assemblage formed by the trapping of a pocket of melt. The ovoid outer envelope of the schreibersite (shown dashed in Fig. 3b) defines the size of the melt-filled pocket at the point when schreibersite became a liquidus phase and began crystallizing on the wall of the chamber. Continued crystallization resulted in the FeS-rich melt being confined to interior regions of the original chamber, with FeS eventually crystallizing there.

Malvin et al. (1984) investigated a set of 12 samples sawed from a bar removed from the same Santa Luzia slab; its approximate position is shown on Fig. 3b. Unfortunately, we did not document the sample with a photo nor with

detailed notes. We infer that the samples were numbered from bottom to top. Although the bar passed directly through the large schreibersite-troilite assemblage, we analyzed only one massive schreibersite sample (position 4) and one troilite (position 12) sample; the remaining ten samples were metal. The analyzed troilite does not appear on Figs. 3a,b; it apparently outcropped on the opposite side of the slab.

After cutting the bar into prisms some of the metal samples appeared to be pure (swathing) kamacite (kam) sprinkled with tiny rhabdites, whereas others (nos. 5, 8, and 9) contained moderate amounts of schreibersite. In the latter case a dental drill was used to remove as much schreibersite as practical.

Data for several elements are plotted in Fig. 13; some were multiplied by factors to allow the diagram to be more compact. Concentration variations are small among the metal samples. The largest apparent variations are in Ir, but these mainly reflect the high uncertainties (∼20% relative) at these low (ca. 0.013 μg/g) concentration levels.

The Ni concentration in the schreibersite is near the center of the range observed in massive schreibersite (schr) in Santa Luzia by Clarke and Goldstein (1978). After Ni the element with the highest schr/kam ratio is W; its concentration in schreibersite is only about 30% lower than in kamacite. Next is Co, 2.5× lower in schreibersite than in kamacite.

The Ni variations in kamacite (top curve of Fig. 13) show the typical values expected (50–60 mg/g); the slightly higher values at positions 7, 8, and 11 probably reflect

small amounts of contamination by schreibersite. In samples 3 and 5 adjacent to massive schreibersite the concentrations of Ni, Au, and Ir seem to be lower and the concentrations of Co higher than in samples more distant from schreibersite.

The Ni content of the "troilite" is much too high; the expected value is <5 mg/g; it therefore appears that about 20% of the sample was schreibersite. The Cr content is 300× higher than in the metal; this is probably now mainly present as daubreelite (although Buchwald did not find this phase). The high Cr content demonstrates that the Cr content of the trapped melt was very high, and thus that D_{Cr} was much lower than unity. The Cu content of the troilite is twice that in the metal; if we assume that most of the Cu in the trapped melt ended up in the troilite, D_{Cu} must have been ∼1.

The only other element for which we obtained troilite data was Au (the Au detection limit is lower and the data are more precise than for other trace elements); the fact that the As, W, and Ir values are shown going off scale represents our present-day inference regarding their detection limits for this INAA run. Despite the fact that the Au concentration was high in the trapped melt, its concentration in schreibersite and troilite are very low. Presumably D_{Au} became much larger than unity as the trapped melt crystallized, and the last metal had enhanced Au concentrations compared to the first metal to crystallize from the trapped melt pocket. There appears to be a significant increase in Au through samples 8, 9, 10, and 11, perhaps a reflection of this effect that was not fully erased by later metamorphic diffusion and minor redistribution during the impact-induced shear discussed by Buchwald (1975).

Appendix B. Replicate data and paired specimens

In Table EA3 in the electronic annex and, for paired irons, Table A1 (duplicated in Table EA2) we list individual analyses of IIAB irons carried out after 1980 (earlier for a few paired irons). Columns two and three give the year and month of the analysis. As discussed in the experimental section, early INAA runs that did not include a Filomena standard and were not cut to uniform thicknesses have been reevaluated. In most cases, we were able to use two or more of the analyzed specimens as "proxy standards" based on more recently analyzed replicates for those irons. As a result, these early data are only slightly less precise than the more recent results. Nonetheless, recent analyses were give double weight in the determination of the means.

Some of the data show evidence of contamination, such as large disagreements between replicate values. For example, the two As values of both Cincinnati and Pima County differ by a factor around 1.4. On plots (e.g., Ir–As) even the lower values appear to be about 20% too high; we therefore did not include the As values in Table 1 nor these meteorites on diagrams involving As.

Most of the Avce data are too high. This was a very thin sample, and had been heavily etched. We suspect that Fe
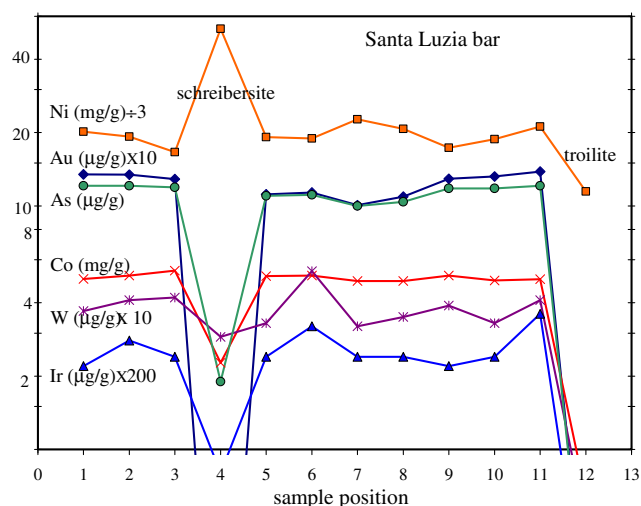

Fig. 13. Siderophile concentrations along a bar cut from Santa Luzia specimen 1618 from the Smithsonian Institution. Concentrations are multiplied or divided by the listed factors to make the diagram more compact, and thus the variation in each element more easily recognized. Most elements show nearly constant concentrations in the metal, but (well determined) Au seems to be slightly higher near the troilite. The enhancement of Ni in schreibersite is well known; the only other elements showing appreciable concentrations in this phase are W and Co. The high Ni content of the "troilite" implies that it also contains appreciable schreibersite; contents of other elements are very low.

Table A1
Replicate values of paired meteorites and regions within the Old Woman meteorite

Meteorite	Yr	mo	Cr	Co	Ni	Cu	Ga	As	W	Re	Ir	Pt	Au
Ainsworth	99	11	30	5.03	55.5	105	52.5	9.38	0.70	<40	0.023	4.5	1.007
Ainsworth	99	12	33	4.98	56.7	107	54.3	9.19	0.69	<20	0.026	4.3	1.033
Ainsworth (Central Mo.)	00	2	30	4.86	60.9	113	52.4	9.20	0.65	<25	0.023	3.4	1.044
Ainsworth (Central Mo.)	00	4	30	4.63	70.9	129	53.5	9.00	0.59	<30	0.016	4.7	1.121
Ainsworth (Ponca Creek)	99	12	33	4.77	62.5	118	56.3	9.45	0.62	<30	0.020	4.3	1.094
Ainsworth (Ponca Creek)	00	2	35	4.79	61.9	115	53.3	9.25	0.61	<32	0.026	3.4	1.078
Pirapora	76	11	109	4.41	56.5	136	57.2	3.51	3.38	2880	27.2		0.535
Pirapora	77	1	111	4.55	56.3		60.0	3.74	3.51	2734	30.9		0.524
Pirapora	02	12	88	4.51	52.5	138	59.8	3.92	3.55	3250	31.6	34.4	0.520
Pirapora (Angra d.Reis)	77	1	<100	4.47	55.7		57.4	3.69	3.35	2665	30.8		0.537
Pirapora (Angra d.Reis)	77	9	163	4.44	52.0	131	54.6	3.36	3.42	2440	26.5		
Pirapora (Angra d.Reis)	02	12	79	4.53	52.2	136	57.7	3.99	3.57	3021	31.4	33.2	0.517
Mejillones	00	4	48	4.63	54.6	129	60.1	5.14	2.23	88	1.92	20.4	0.665
Mejillones	00	6	307	4.61	54.8	130	59.3	5.18	2.20	165	1.91	18.0	0.661
Mejillones (Elqui)	90	3	1040	4.54	59.8	137	57.7	5.13	2.15	140	1.90	16.8	0.655
Mejillones (Elqui)	90	4	156	4.57	59.8	136	61.0	5.34	2.18	<300	1.99	17.8	0.666
Old Woman	76	11	45	4.41	61.1	117	56.3	5.10	2.00	58	0.750		0.683
Old Woman	77	1	<120	4.60	58.9		56.8	4.96	1.90	<180	0.873		0.682
Old Woman H	96	4	43	4.60	55.5	124	56.3	5.22	2.09	<90	0.826	13.7	0.676
Old Woman H	00	8	45	4.66	57.0	122	56.8	5.42	2.06	33	0.803	15.0	0.687
Old Woman Ogg	96	4	50	4.67	53.5	133	56.5	5.46	1.93	<120	0.837	15.7	0.687
Old Woman Ogg	00	8	49	4.72	55.5	121	58.5	5.82	2.10	56	0.835	16.4	0.704
Richland (Fredericksburg)	00	8	94	4.59	55.9	138	58.6	4.48	2.93	663	8.51	25.8	0.579
Richland (Fredericksburg)	00	9	88	4.56	54.4	129	58.1	4.27	2.73	669	8.37	24.5	0.571
Richland	00	8	37	4.55	56.6	127	58.7	4.60	2.65	579	8.41	27.7	0.589
Richland	00	9	36	4.57	55.4	122	60.5	4.69	2.84	737	8.62	25.5	0.584
Santa Luzia	83	12a	15	5.20	55.3	104	43.5	9.86	0.31		0.013		1.215
Santa Luzia	02	10	16	5.06	59.6	110	45.6	11.9	0.32	<30	0.013	2.9	1.302
Santa Luzia(MinasGer.)	77	9	<50	5.34	56.7	117	50.0	12.4	0.36	<89	<0.045		1.412
Sikhote-Alin	87	9	31	4.83	59.8	118	53.8	9.20	0.73	<21	0.029	5.2	1.074
Sikhote-Alin (Dutch Flat)	03	2	31	4.92	57.6	115	54.9	8.93	0.82	<45	0.021	6.1	1.025
Sikhote-Alin (Dutch Flat)	03	4	46	4.86	57.9	109	56.1	9.15	0.81	<53	0.020	4.4	1.034

Concentrations are μg/g except Co and Ni (mg/g) and Re (ng/g).

and Co, both concentrated in kamacite, had been selectively lost, thus raising all other elements. In other groups As is higher in kamacite relative to taenite; in contrast, As also seems to be slightly enhanced in Avce. As discussed below for Ainsworth, there is some evidence that As behaves differently in group IIAB.

In Table A1 we list multiple replicates for different structural portions of the Old Woman meteorite and for several sets (Ainsworth, Mejillones, Para de Minas, Richland, Santa Luzia, and Sikhote-Alin) of (probably) paired IIAB irons. We could not resolve differences in the metal composition of the hexahedrite (H) and coarsest-octahedrite (Ogg) structures in the Old Woman iron. We visually examined the large section of this meteorite at the Smithsonian Institution and found that the structural differences are quite subtle; the kamacite is only slightly coarser in the H regions relative to the Ogg regions. In our opinion, these regions are too similar to warrant separate analysis.

There are resolvable differences in the Ainsworth data set. Especially noteworthy are the anticorrelated Co and Ni variations. However, as noted above in connection with Fig. 1g, such differences can reflect small stochastic differences in the abundance of the rare taenite phase; the kamacite/taenite concentration ratio is about 6 for Co and about

0.1 for Ni. There is no resolvable correlation of As with Co, as expected if As were significantly enriched in kamacite compared to taenite. Ainsworth-Ponca Creek has low mean Co but the highest mean As. As discussed in connection with Avce, the different chemistry (higher degree of reduction) or inclusion content (uniformly high content of schreibersite grains large and small) may be changing the detailed distribution of As in the mineral mix in the analyzed samples.

The Mejillones Ni-poor ataxite originated in the Atacama Desert of Chile. Its present texture was formed by a combination of impact-induced structural damage followed by annealing/recrystallization (Buchwald, 1975). The provenance of the Elqui iron is unknown; it was characterized and named by Wasson and Canut de Bon (1998), who described the structure as that of a hexahedrite containing rhabdites. It was stated that "its composition is different from that of any other Chilean IIAB". This statement is incorrect; the composition is identical to that of the Mejillones Ni-poor ataxite. Probably the authors neglected to make the comparison because of the perceived structural difference. We have reexamined the structure of our small (1.5 cm^2) UCLA section of Elqui. It does not contain recognizable rhabdites; instead, it shows evidence

of reheating and resorption of rhabdites. However, the structure is quite different from the detailed textures illustrated by Buchwald (1975) for Mejillones; he observed numerous large rhabdites as well as a granular texture. Because impact heating can leave very different records over distances of centimeters, our present (but still tentative) conclusion is that Elqui should be paired with Mejillones. It might also be that the small Elqui specimen has experienced artificial reheating. We continue to list it in Table 1 but do not plot it on our diagrams.

The small (48-g) Dutch Flat iron was reportedly discovered by gold prospectors in the Arizona desert. The type specimen at UCLA was obtained from Rob Matson, who obtained the meteorite from the finders. As the data in Table 2 make clear, its composition is unresolvable from the widely distributed Sikhote-Alin iron, nuggets of which are frequently sold at gem-and-mineral shows. We list it as an independent iron in Table 1 and did not plot it on our diagrams. However, because of its tiny size and close compositional resemblance to Sikhote-Alin we suggest that the most practical approach is to treat it as paired unless and until future studies (e.g., of cosmic-ray produced isotopes) show that it is probably an independent fall.

The 47-kg Fredericksburg (Texas) iron was first reported to us by a person living in Alaska, who stated that it had been inherited from a deceased relative who had lived near Fredericksburg. Our analysis of the sample shows that, within error, its composition is the same as that of the Richland (Texas) iron. Both irons appear to be strongly weathered. However, these two Texas locations are 297 km apart, farther apart than plausible for a strewn field. Our best guess is that human transport has been involved, and that they are fragments from the same fall event. Fredericksburg is not an approved name; we suggest that this mass be referred to as Richland (Fredericksburg) unless future studies imply that it resulted from a distinct fall.

As suspected by Buchwald (1975) and confirmed already by Kracher et al. (1980), Angra dos Reis (iron) is the same as Pirapora. In Table A1 we list some very early data from the 1970s as well as a new analysis of each iron that confirms their identical compositions.

For the past two decades each of our irradiations has included a sample of National Bureau of Standards standard steel NBS 809B and of the IIAB North Chile hexahedrite; with rare exceptions the latter samples were taken from the Filomena specimen housed at the Smithsonian Institution. Since 1997 all irradiations have also included a sample of the IIAB hexahedrite Coahuila, which is useful because of its high content of refractory siderophiles.

In Tables EA4a,b,c in the electron annex we list replicate data for our three standards together with sample standard deviations calculated from these data. We do not include data for elements having concentrations near our detection limits since these are not useful for quantitative calibra-

tions. The one exception is for Ir in NBS 809B which we justify because Ir is an important element and this is a widely distributed standard.

These data provide two kinds of useful information. They provide our best estimates of the mean compositions. Absolute calibrations have not been attempted, thus errors as large as 5% may be present in some elements. More importantly, they document the degree of elemental reproducibility of the standards. This is important because a neutron activation standard needs to be uniform (the other key need is that the concentration be much higher than the detection limit).

Appendix C. Supplementary data

Supplementary data associated with this article can be found, in the online version, at doi:10.1016/j.gca.2006.09.032.

References

Afiattalab, F., Wasson, J.T., 1980. Composition of the metal phases in ordinary chondrites: implications regarding classification and metamorphism. *Geochim. Cosmochim. Acta* **44**, 431–446.

Brandes, E.A., Brook, G.B., 1998. *Smithells Metal Reference Book*. Butterworth-Heinemann, CA, pp. 1600.

Buchwald, V.F., 1975. *Handbook of Iron Meteorites*. University of California Press, pp. 1418.

Chabot, N.L., 2004. Sulfur contents of the parental metallic cores of magmatic iron meteorites. *Geochim. Cosmochim. Acta* **68**, 3607–3618.

Chabot, N.L., Drake, M.J., 2000. Crystallization of magmatic iron meteorites: the effects of phosphorus and liquid immiscibility. *Meteorit. Planet. Sci.* **35**, 807–816.

Chabot, N.L., Jones, J.H., 2003. The parameterization of solid metal-liquid metal partitioning of siderophile elements. *Meteorit. Planet. Sci.* **38**, 1425–1436.

Chabot, N.L., Campbell, A.J., Jones, J.H., Humayun, M., Lauer, H.V., 2006. The influence of carbon on trace-element partitioning behavior. *Geochim. Cosmochim. Acta* **70**, 1322–1335.

Clarke, R., Goldstein, J., 1978. Schreibersite growth and its influence on the metallography of coarse-structured iron meteorites. *Smithson. Contrib. Earth Sci.* **21**, 1–80.

Cook, D.L., Walker, R.J., Horan, M.F., Wasson, J.T., Morgan, J.W., 2004. Pt–Re–Os systematics of group IIAB and IIIAB iron meteorites. *Geochim. Cosmochim. Acta* **68**, 1413–1431.

Esbensen, K.H., Buchwald, V.F., Malvin, D.J., Wasson, J.T., 1982. Systematic compositional variations in the Cape York iron meteorite. *Geochim. Cosmochim. Acta* **46**, 1913–1920.

Frondel, C., Klein, C., 1965. Ureyite, $NaCrSi_2O_6$: A new meteorite pyroxene. *Science* **149**, 742–743.

Haack, H., Scott, E.R.D., 1993. Chemical fractionations in group IIIAB iron meteorites: origin by dendritic crystallization of an asteroidal core. *Geochim. Cosmochim. Acta* **57**, 3457–3472.

Jones, J.H., Drake, M.J., 1983. Experimental investigations of trace element fractionations in iron meteorites, II: the influence of sulfur. *Geochim. Cosmochim. Acta* **47**, 1199–1209.

Jones, J.H., Malvin, D.J., 1990. A nonmetal interaction model for the segregation of trace metals during solidification of Fe–Ni–S, Fe–Ni–P, and Fe–Ni–S–P alloys. *Metall. Trans. b* **21**, 697–706.

Kracher, A., Wasson, J.T., 1982. The role of S in the evolution of the parental cores of the iron meteorites. *Geochim. Cosmochim. Acta* **46**, 2419–2426.

Kracher, A., Willis, J., Wasson, J.T., 1980. Chemical classification of iron meteorites–IX. A new group (IIF), revision of IAB and IIICD, and data on 57 additional irons. *Geochim. Cosmochim. Acta* **44**, 773–787.

Malvin, D.J., Wang, D., Wasson, J.T., 1984. Chemical classification of iron meteorities-X. Multielement studies of 43 irons, resolution of group IIIE from IIIAB, and evaluation of Cu as a taxonomic parameter. *Geochim. Cosmochim. Acta* **48**, 785–804.

Nagamori, M., 1969. Density of molten Ag–S, Cu–S, Fe–S, and Ni–S systems. *Trans. Metall. Soc. AIME* **245**, 1897–1902.

Raghavan, V., 1988. The Fe–P–S system. In Ternary Systems Containing Iron and Sulphur, pp. 209–217.

Schaudy, R., Wasson, J.T., Buchwald, V.F., 1972. The chemical classification of iron meteorites-VI. A reinvestigation of irons with Ge concentrations lower than 1 ppm. *Icarus* **17**, 174–192.

Schürmann, E., Neubert, V., 1980. Schmelzgleichgewichte in den eisenreichen Ecken der Dreistoffsysteme Eisen-Schwefel-Kohlenstoff, Eisen-Schwefel-Phosphor und Eisen-Schwefel-Silicium. *Giessereiforschung* **32**, 1–5.

Scott, E.R.D., 1972. Chemical fractionation in iron meteorites and its interpretation. *Geochim. Cosmochim. Acta* **36**, 1205–1236.

Scott, E.R.D., 1977. Geochemical relationships between some pallasites and iron meteorites. *Mineral. Mag.* **41**, 265–272.

Ulff-Møller, F., 1998. Effects of liquid immiscibility on trace element fractionation in magmatic iron meteorites: a case study of group IIIAB. *Meteorit. Planet. Sci.* **33**, 207–220.

Wasson, J.T., 1969. The chemical classification of iron meteorites-III. Hexahedrites and other irons with germanium concentrations between 80 and 200 ppm. *Geochim. Cosmochim. Acta* **33**, 859–876.

Wasson, J.T., 1999. Trapped melt in IIIAB irons; solid/liquid elemental partitioning during the fractionation of the IIIAB magma. *Geochim. Cosmochim. Acta* **63**, 2875–2889.

Wasson, J.T., Kallemeyn, G.W., 1988. Compositions of chondrites. *Philos. Trans. R. Soc. London A* **325**, 535–544.

Wasson, J.T., Kallemeyn, G.W., 2002. The IAB iron–meteorite complex: a group, five subgroups, numerous grouplets, closely related, mainly formed by crystal segregation in rapidly cooling melts. *Geochim. Cosmochim. Acta* **66**, 2445–2473.

Wasson, J.T., Canut de Bon, C., 1998. New chilean iron meteorites: medium octahedrites from northern Chile are unique. *Meteorit. Planet. Sci.* **33**, 175–179.

Wasson, J.T., Choi, B.-G., 2003. Main-group pallasites—chemical composition, relationship to IIIAB irons, origin. *Geochim. Cosmochim. Acta* **67**, 3079–3096.

Wasson, J.T., Huber, H., 2006. Compositional trends among IID irons; their possible formation from the P-rich lower magma in a two-layer core. *Geochim. Cosmochim. Acta* **70**, 6153–6167.

Wasson, J.T., Lange, D.E., Francis, C.A., Ulff-Møller, F., 1999. Massive chromite in the Brenham pallasite and the fractionation of Cr during the crystallization of asteroidal cores. *Geochim. Cosmochim. Acta* **63**, 1219–1232.

Wasson, J.T., Matsunami, Y., Rubin, A.E., 2006. Silica and pyroxene in IVA irons; possible formation of the IVA magma by impact melting and reduction of L-LL-chondrite materials followed by crystallization and cooling. *Geochim. Cosmochim. Acta* **70**, 3149–3172.

Wasson, J.T., Ouyang, X., Wang, J., Jerde, E., 1989. Chemical classification of iron meteorites: XI. Multi-element studies of 38 new irons and the high abundance of ungrouped irons from Antarctica. *Geochim. Cosmochim. Acta* **53**, 735–744.

Wasson, J.T., Richardson, J.W., 2001. Fractionation trends among IVA iron meteorites: contrasts with IIIAB trends. *Geochim. Cosmochim. Acta* **65**, 951–970.